

MANIPULATION OF ANIMAL GROWTH BY SUPPRESSING THE FUNCTIONS
OF GROWTH DIFFERENTIATION FACTORS 8 (MYOSTATIN) AND 11
WITH THEIR PROPEPTIDES

A DISSERTATION SUBMITTED TO THE GRADUATE DIVISION OF THE UNIVERSITY
OF HAWAI'I AT MÂNOA IN PARTIAL FULFILLMENT OF THE REQUIREMENTS FOR
THE DEGREE OF

DOCTOR OF PHILOSOPHY

IN

MOLECULAR BIOSCIENCES AND BIOENGINEERING

DECEMBER 2010

BY

Zicong Li

Dissertation Committee:

Jinzeng Yang, Chairperson

Stefan Moisyadi

Yong Soo Kim

Ching Yuan Hu

Scott Lozanoff

ACKNOWLEDGMENTS

My most grateful and sincere thanks

To Dr. Jinzeng Yang for his financial support, for his patient guidance and critical comments on my research, for sharing his expertise, knowledge, thoughts and perspectives in the field of animal biotechnology and growth biology, and for his great encouragement, help and care during all my studies at University of Hawai‘i.

To Dr. Dulal Borthakur, for accepting me in the MBBE program, for his continuous encouragement, fundamental help and support during all my studies at University of Hawai‘i.

To Dr. Stefan Moisyadi, for helping me to produce the GDF11 propeptide transgenic mice, for his critical review and suggestions to my research proposals and manuscripts, for sharing his expertise and knowledge in the field of transgenesis, and for serving in my dissertation committee.

To Dr. Yong Soo Kim, for helping me to analyze the inhibition of myostatin by recombinant pig myostatin propeptide in A204 cells, for allowing me to use his lab, for his critical review and suggestions to my research proposals and manuscripts, for sharing his expertise and knowledge in the field of myostatin and muscle biology, and for serving in my dissertation committee.

To Dr. Ching Yuan Hu, for his critical review and suggestions to my research proposals and manuscripts, for sharing his expertise and knowledge in the field of animal growth biology, and for serving in my dissertation committee.

To Dr. Scott Lozanoff, for his critical review and suggestions to my research proposals and manuscripts, for sharing his expertise and knowledge in the field of bone biology and metabolism, and for serving in my dissertation committee.

To Mrs. Baoping Zhao for her technical support and critical suggestions to my research, for her great help and care during all my studies at University of Hawai‘i.

To Miyuri Kawasumi, Heng Wang, Yanisa Thai-u-laoong, Shizu Watanabe, Gang Pan for their help on my research and their friendships during all my studies at University of Hawai‘i.

To Dr. Zhenfang Wu, my Master’s advisor, a professor at South China Agricultural University, for his great support to my graduate admission application to University of Hawai‘i, his continuous encouragement, enlightening advice during all my studies at University of Hawai‘i.

To my father Guoxin Li (*in memoriam*), my mother Huafang Liang, my brother Ziming Li, my girlfriend Fang Zeng for their love, encouragement and support during all my studies at University of Hawai‘i.

ABSTRACT

Muscle growth and bone growth are important for meat production as well as human health, since muscle and bone are two major body components in agricultural animals and abnormal development of the musculoskeletal system, which is formed by muscles and bones, will cause serious health problems to humans. Growth differentiation factor 8 (GDF8, also called myostatin) is a remarkable inhibitor for muscle growth, and growth differentiation factor 11 (GDF11) is a significant regulator that controls normal formation of skeletons. Myostatin and GDF11 are two highly homologous molecules that are antagonized by their own propeptide, myostatin propeptide and GDF11 propeptide, through a similar mechanism. Myostatin propeptide and GDF11 propeptide are generated from the N-terminal peptide present in the myostatin precursor and GDF11 precursor, respectively, following proteolytic processing. Mouse myostatin propeptide has been shown to promote muscle growth by blocking myostatin function. A mutated mouse myostatin propeptide carrying a mutation at the cleavage site of the BMP-1/TLD-like metalloproteinases was recently demonstrated to be more effective in promoting muscle growth than the wild-type mouse myostatin propeptide. GDF11 propeptide also was recently shown to antagonize GDF11 function in vitro. This project was designed to study the effect of a BMP-1/TLD-like metalloproteinases-resistant pig myostatin propeptide (a mutated pig myostatin propeptide) on muscle growth by depressing myostatin function, and the effects of mouse GDF 11 propeptide on bone growth by antagonizing GDF11 function.

Recombinant wild-type and mutated porcine myostatin propeptides were produced in insect cells. Their purities and identities were confirmed by SDS-PAGE and Western Blot with anti-his.tag and anti-myostatin propeptide antibodies. Using the A204 cells reporter assay system, the abilities to depress myostatin activity in vitro were compared between wild-type and mutated pig

myostatin propeptide. In 6h co-incubation analysis, mutated and wild-type porcine myostatin propeptides showed no difference in blocking myostatin activity, while in 24 h or 48 h co-incubation analyses, the former had a stronger effect on blocking myostatin activity than the later, suggesting the mutated pig myostatin propeptide has increased resistance to the degradation by BMP-1/TLD-like metalloproteinases. The mutated porcine myostatin propeptide was injected into neonatal mice to test its *in vivo* effects on muscle growth. Mice treated with mutated propeptide were 11–15% heavier than the controls from the age of 25 to 57 days. The weights of major skeletal muscles significantly increased by 13.5–24.8% in mice injected with mutated pig myostatin propeptide. Muscle histology analysis showed that enhanced muscle mass in mice administered with mutated pig myostatin propeptide was primarily caused by increase of muscle fiber size. These results indicate that the pig myostatin propeptide also is inhibited by the BMP-1/TLD-like metalloproteinases, the mutated pig myostatin propeptide may have application for improving muscle growth in pigs.

To investigate the *in vivo* effects of GDF11 propeptide on bone growth by suppressing GDF11 function, transgenic mice over-expressing GDF11 propeptide specifically in bone tissue were generated by intracytoplasmic sperm injection (ICSI) in combination with piggyBac transposon-mediated gene transfer. Skeletal analyses showed that transgenic mice exhibited transformation of the seventh cervical vertebra (C7) into a thoracic vertebra, since extra ribs were formed on the C7 of transgenic mice. The effect of GDF11 propeptide transgene on forming the C7 ribs depended on transgene expression level, as the frequency of forming the C7 ribs was associated with the transgene mRNA abundance in transgenic mice. Reverse transcription PCR revealed that the transgene started to express at 12.5 dpc or between 10.5-12.5 dpc in transgenic mice. Altered expression patterns of *Hoxa-4* and *Hoxa-5* genes were found in

13 dpc transgenic mice by in situ hybridization, suggesting the transgene signals through these two Hox genes to regulate vertebral patterning. Earlier ossification was observed in 16.5 dpc transgenic mice, in comparison with wild-type littermates. X-rays analysis and bone histology analysis showed that bone mineral content, bone mineral density and relative trabecular bone volume were significantly increased by 11.12%, 9.68% and 60.9%, respectively, in adult transgenic male mice, and 14.96%, 8.69% and 57.7%, respectively, in adult female transgenic mice, compared to their sex-matched wild-type littermates. These results reveal that GDF11 propeptide plays an important role in vertebral formation and postnatal bone growth.

The overall results of this study enhanced our understanding on regulation of muscle growth and bone growth by myostatin, GDF11 and their propeptides. The knowledge obtained from this work supports further studies that aim to manipulate agricultural animal growth or improve human health.

TABLE OF CONTENTS

Acknowledgements.....	ii
Abstract.....	iv
List of tables.....	xii
List of figures.....	xiii
Chapter 1. Introduction	
1.1. Project overview.....	1
1.2. Muscle formation.....	2
1.3. Muscle metabolism and muscle fiber types.....	3
1.4. Regulation of muscle growth.....	4
1.5. Myostatin and muscle growth.....	5
1.6. Bone formation.....	7
1.7. Bone and calcium metabolism.....	8
1.8. Regulation of bone growth.....	9
1.9. GDF11 and bone growth.....	10
1.10. Regulation of the activities of myostatin and GDF11 by their own propeptides...11	
1.11. Hypotheses and research objectives.....	12

Chapter 2. Suppression of myostatin by a mutated pig myostatin propeptide

2.1. Abstract.....	14
2.2. Introduction.....	15
2.3. Materials and methods.....	17
2.3.1. Plasmid construction and preparation.....	17
2.3.2. Cell culture and transfection.....	18
2.3.3. Protein expression and purification.....	18
2.3.4. SDS-PAGE and Western Blotting analyses.....	19
2.3.5. pGL3-(CAGA) ₁₂ -luciferase reporter assay in A204 rhabdomyosarcoma Cells.....	20
2.3.6. Administration of propeptide to neonatal mice.....	21
2.3.7. Determination of muscle fiber size.....	21
2.3.8. Statistical analysis.....	22
2.4. Results.....	22
2.4.1. Production of wild-type and mutated porcine myostatin propeptides from insect cells.....	22
2.4.2. Effects of wild-type and mutated propeptide on blocking myostatin activity	

in vitro.....	23
2.4.3. Administration of mutated propeptide to neonatal mice significantly increased muscle growth.....	24
2.5. Discussion and conclusions.....	25
Chapter 3. Suppression of growth differentiation factor 11 by transgenic over-expression of its propeptide in skeleton	
3.1. Abstract.....	36
3.2. Introduction.....	37
3.3. Materials and Methods.....	38
3.3.1. Construction of transgene plasmid and production of transgenic mice.....	38
3.3.2. Identification of transgenic mice.....	39
3.3.3. Analyses of transgene expression.....	40
3.3.4. Alizarin red and alcian blue staining of skeleton.....	41
3.3.5. In situ hybridization.....	41
3.3.6. Analysis of ossification in embryos.....	42
3.3.7. X-ray analyses of body composition and bone mineral.....	42
3.3.8. Measurement of the length of forelimb bones.....	42
3.3.9. Histology analysis of bone volume.....	42

3.3.10. Statistical analysis.....	43
3.4. Results.....	43
3.4.1. Production of transgenic mice.....	43
3.4.2. Expression of transgene in transgenic mice.....	43
3.4.3. Skeletal abnormalities in transgenic mice.....	44
3.4.4. Expressions of Hoxa-4 and Hoxa-5 genes in transgenic mice.....	46
3.4.5. Ossification in transgenic mice.....	47
3.4.6. Body mass, muscle mass, total bone mineral content, bone area and bone mineral density in transgenic mice.....	47
3.4.7. Increase of bone volume in transgenic mice.....	48
3.4.8. The length of bones in forelimb of transgenic mice.....	48
3.5. Discussion and Conclusions.....	48

Chapter 4. General discussion and conclusions

4.1. General discussion.....	64
4.2. Conclusions.....	66
4.3. References.....	68
4.4. Appendices.....	87

4.4.1. Appendix A: The raw data of Table 2.1.....	87
4.4.2. Appendix B: The raw data of Figure 2.3.....	90
4.4.3. Appendix C: The raw data of Figure 2.4.....	92
4.4.4. Appendix D: The raw data of Figure 2.5.....	93
4.4.5. Appendix E: The raw data of Figure 2.6.....	96
4.4.6. Appendix F: The raw data of Table 3.2.....	98
4.4.7. Appendix G: The raw data of Figure 3.7.....	100

LIST OF TABLES

Table	Page
Table 2.1 Muscle weights of mice injected with mutated pig myostatin propeptide or PBS.....	28
Table 3.1 Skeletal analysis of wild-type and transgenic littermates from different lines.....	52
Table 3.2 Body mass, muscle mass, total bone mineral content, bone area and bone mineral density of 10 week-old wild-type mice and their transgenic littermates.....	53
Table 3.3 Length of the ulna bone and the humerus bone in forelimb of 10 week-old wild-type mice and their transgenic littermates.....	54

LIST OF FIGURES

Figure	Page
Figure 2.1 Transfection efficiency of recombinant protein expression plasmid in sf9 insect cells.....	29
Figure 2.2 Production of wild-type and mutant form of porcine myostatin propeptide from insect cells.....	30
Figure 2.3 Inhibition of myostatin activity (20ng/ml) by different concentrations of wild-type or mutated pig myostatin propeptide after 6h co-incubation in A204 cells.....	31
Figure 2.4 Inhibition of 20ng/ml of myostatin by 100ng/ml of wild-type or mutated pig myostatin propeptide after 6h, 24h and 48h co-incubation in A204 cells.....	32
Figure 2.5 Growth curves of mice after injection with mutated pig myostatin propeptide or PBS.....	33
Figure 2.6 Muscle histology analyses of mice injected with mutated pig myostatin propeptide or PBS.....	34
Figure 3.1 Production of transgenic mice.....	55
Figure 3.2 Expression of transgene in transgenic mice.....	56
Figure 3.3 Abnormalities in the anterior/posterior axial skeleton of transgenic mice.....	58
Figure 3.4 Changes in morphological appearance of the seventh cervical vertebra in transgenic mice.....	59

Figure 3.5 Altered expression patterns of Hoxa-4 and Hoxa-5 genes on the anterior/posterior axis
in transgenic mice.....60

Figure 3.6 Advanced ossification in transgenic mice.....61

Figure 3.7 Increase of trabecular bone volume in transgenic mice.....62

CHAPTER 1

INTROUCTION

1.1. Project overview

Meat production in agricultural animals is mainly determined by muscle growth, since muscle tissue is the major component of meat. Meat production also is affected by bone growth, as muscles are attached to bones and hence bone growth indirectly affects muscle mass by determining muscle length. Therefore, promoting muscle growth as well as bone growth in meat-producing animals is likely to improve the efficiency of meat production.

Furthermore, normal development of muscles and bones are important for human health, since muscles together with skeletons form the musculoskeletal system that not only provides shape, support, movement and protection for the body, but also is the important site for body metabolism. Abnormal development of the musculoskeletal system results in defects in appearance and function of the body, causing serious health problems to humans. Hence, understanding the mechanisms that regulate the growth of muscles and bones may help us to develop strategies for manipulating meat animal growth as well as treating human musculoskeletal diseases.

Muscle growth and bone growth are regulated by a group of growth factors, such as the well-known insulin-like growth factor-1 (IGF-1) . Recently, two highly homologous members of the transforming growth factor- β (TGF- β) superfamily, growth differentiation factor -8 (GDF8, also called myostatin) and -11 (GDF11), have been identified to play remarkable roles in muscle growth and bone development, respectively. Myostatin normally acts to limit muscle growth (McPherron et al., 1997) while GDF11 is essential for normal skeletal formation and

development (McPherron et al., 1999; Gamer et al., 2001). Beside the high homology between them, the activities of myostatin and GDF11 are regulated in a very similar manner. Both of them are down-regulated by the N-terminal peptides present in their own precursor proteins, which are called myostatin propeptide and GDF11 propeptide, respectively (Yang et al., 2001; Ge et al., 2005). The objectives of the present study were 1) To investigate the effects of blocking myostatin function with administered pig myostatin propeptide on muscle growth in mice; 2) To study the functions of GDF11 propeptide in bone formation and development by using transgenic mouse over-expressing GDF11 propeptide in skeleton as a model.

1.2. Muscle formation

During the early embryonic stage, muscle progenitor cells from mesoderm-derived somites express myogenic regulatory factors (MRFs), including MyoD, Myf5, myogenin and MRF4, which are a group of transcription factors that contain a conserved E-box DNA-binding domain (Weintraub et al., 1991; Perry and Rudnick, 2000). Expressions of these myogenic transcription factors induce differentiation of muscle stem cells into myoblasts. Cells producing a myogenic transcription factor are committed to becoming muscle cells, since transfection of genes encoding any of these myogenic proteins into various cultured cells convert those cells into myoblasts (Thayer et al. 1989; Weintraub et al. 1989).

Once myoblasts are formed, they start to proliferate in the presence of some particular growth factors, especially fibroblast growth factor. When these growth factors cease expression, myoblasts stop division, secrete fibronectin onto their extracellular matrix to trigger fusion of myoblasts into multinuclear myofiber (Boettiger et al. 1995). Following secretion of fibronectin, myoblasts align together into chains. This step is regulated by cell membrane glycoproteins

(Knudsen 1985). After several myoblasts join together, the adjoining cell membranes start to dissolve, resulting in merging of aligned myoblasts into multinuclear myofibers. Calcium ions are believed to be critical for the fusion of myoblasts, as this process can be activated by calcium ionophores that carry calcium ions across cell membranes (David et al. 1981). Myoblast fusion also appears to be mediated by a group of metalloproteinases called meltrins, which are highly homologous to fertilin, a protein that regulates sperm-egg membrane fusion. (Yagami-Hiromasa, 1995). According to the time of formation, myofibers are divided into primary myofibers, which are formed in the first wave of myogenesis, and secondary myofibers, which are formed in the second wave of myogenesis following the formation of primary myofibers. Secondary myofibers results from proliferation, alignment, and fusion of secondary myoblasts which had remained quiescent. Primary myofibers serve as scaffolds for the formation of secondary myofibers, they have peripherally located myofibrils surrounding an axial core of nuclei and cytoplasm (O'Brien et al., 2000; Zhu et al., 2004)

1.3. Muscle metabolism and muscle fiber types

Muscle movement consumes a large proportion of body energy. All muscle fibers utilize glucose to produce ATP to power muscle contraction, but different muscle fibers use different metabolic pathways to generate energy for contraction. Based on their biochemical and physiological properties, muscle fibers can be generally divided into three types, including Type I fibers (also called Slow-twitch oxidative fibers or Red fibers), Type IIA fibers (also known as Fast-twitch oxidative glycolytic fibers or Intermediate fibers) and Type IIB fibers (also referred to as Fast-twitch glycolytic fibers or White fibers) (Gauthier, 1969; Brooke and Kaiser, 1970; Peter et al., 1972). Individual muscles are a mixture of 3 types of muscle fibers, but their proportions depend on the function of that muscle. Type I fibers are characterized by a slow

contraction time and a high resistance to fatigue. Structurally, they have high mitochondrial and capillary density, and high myoglobin content that is responsible for their red color. These fibers use oxidative metabolism to generate ATP for contraction. Muscles mainly containing Type 1 fibers are used for aerobic activities requiring low-level force production, such as walking and maintaining posture. Most daily living activities use these muscles. Type IIB fibers are identified by a quick contraction time and a low resistance to fatigue. They contain a low mitochondrial and capillary density and myoglobin content. They mainly rely on anaerobic glycolysis to generate energy for contraction. Functionally, Type IIB fibers-dominant muscles are used for anaerobic activities with a high force output, such as sprinting and jumping. Type IIA fibers represent a transition between Type 1 and Type IIB fibers. They have the characters of both Type 1 and Type IIB fibers. Since Type II fibers (Including Type IIA and Type IIB fibers) have a higher glycogen concentration and are metabolically better equipped than type I fibers for post-mortem anaerobic glycolysis, which causes changes in color and impairments in water holding capacity of fresh meat, leading to development of pale, soft, and exudative (PSE) meat (Klont et al., 1998). Therefore, a high ratio of Type 1 fibers to Type II fibers in muscles is good for meat quality.

1.4. Regulation of muscle growth

Muscle is composed of numerous muscle fibers, which are formed by fusion of multiple myoblasts. Muscle growth is determined by an increase in muscle fiber number (hyperplasia) as well as an increase in muscle fiber size (hypertrophy). The number of muscle fiber usually is fixed before birth (Luff and Goldspink, 1970; Wegner et al., 2000). Postnatal muscle growth mainly results from muscle hypertrophy. Muscle fiber enlargement could be the consequence of increase in activity of satellite cells, which fuse to adjacent muscle fibers to increase their size.

Satellite cells are undifferentiated muscle precursor cells lying between the basal lamina and the muscle fibers, which are responsible for postnatal growth, repair, and maintenance of skeletal muscle (Seale and Rudnicki, 2000). Enlargement of muscle fiber also could result from elevation in muscle protein synthesis, or decrease in muscle protein degradation, or both. IGF-1, which is activated by growth hormone, stimulates both proliferation and differentiation of myoblasts and satellite cells to regulate muscle growth (Oksbjerg et al., 2004). Furthermore, IGF-1 regulates muscle growth not only by stimulating muscle protein synthesis via the PI3/Akt pathway, but also by suppressing muscle protein breakdown via decreasing expression of ubiquitin-ligases, atrogin-1 and MuRF1 (Romel et al., 2001; Satchek et al., 2004). In addition to IGF-1, steroid hormones, such as testosterone, also stimulate muscle growth by increasing muscle satellite cell numbers and the levels of muscle IGF-I (Dayton and White, 2007). Recently, myostatin, a TGF- β superfamily member, has also been identified as a critical regulator of muscle growth (McPherron et al., 1997).

1.5. Myostatin and muscle growth

Muscle growth is regulated by a group of growth factors. Among them, a member of the transforming growth factor- β (TGF- β) superfamily, growth differentiation factor 8 (GDF8), which is also known as myostatin, is a remarkable negative regulator for muscle growth. Targeted disruption of myostatin caused 100% increase of muscle weight in homozygous mutant mice (McPherron et al., 1997). The enhanced muscle mass in myostatin-deficient mice resulted from increases of both of muscle fiber number and muscle fiber size (McPherron et al., 1997). In contrast, systemic administration of myostatin to adult mice induced profound muscle loss (Zimmers et al., 2002), and transgenic mice over-expressing myostatin had decreased muscle mass (Reisz-Porszasz et al., 2003). Myostatin is highly conserved among many vertebrate

species. The amino acid sequences of mature myostatin protein in mouse, rat, pig, turkey and chicken are 100% while in cattle and sheep are 98.3% identical to that in human (McPherron and Lee, 1997). The function of myostatin also appears conserved across various vertebrate species because loss-of-function natural mutations in myostatin gene have been found to cause dramatic increase of muscle mass in cattle (Grobet et al., 1997; Kambadur et al., 1997; McPherron and Lee, 1997), human (Schuelke et al., 2004), sheep (Clouet et al., 2006) and dog (Mosher et al., 2007).

During embryonic myogenesis, myostatin seems act to inhibit myoblast proliferation and differentiation *via* preventing cell cycle progression and down-regulating the level of myogenic regulatory factors, such as myoD and myogenin (Thomas et al., 2000; Taylor et al., 2001; Langley et al., 2002; Rios et al., 2002). Suppression of myoblast proliferation by myostatin is believed to take place through down-regulating the activity of cyclin D1 at mRNA level as well as protein level, which causes cell cycle arrest at G1 phase (Yang et al., 2006; Ji et al., 2008). After birth, myostatin appears to limit skeletal muscle mass by depressing satellite cell proliferation (McCroskery et al., 2003), and inhibiting muscle protein synthesis in combination with activating muscle protein degradation (McFarland et al., 2006). Inhibition of satellite cell division by myostatin is through decreasing CDK2 protein level in conjunction with up-regulating the activity of CDK inhibitor, p21 (McCroskery et al., 2003). However, some recent studies indicated that activation of satellite cells is not involved in postnatal muscle hypertrophy driven by myostatin blockade, since myostatin suppression-induced hypertrophic muscles contain no more myonuclei or satellite cells than controls (Amthor et al., 2009; Sartori et al., 2009). Myostatin had no significant effect on satellite cell proliferation in vitro, which is believed to be caused by the down-regulation of myostatin receptors in postnatal satellite cells

(Amthor et al., 2009). These findings challenge the generally accepted model of myostatin-based regulation of postnatal muscle growth and suggest that postnatal muscle hypertrophy induced by myostatin blockade probably mainly results from increase in synthesis and turnover of muscle fiber structural proteins rather than enhancement of satellite cell proliferation. Myostatin inhibits Akt phosphorylation, which is required for activating the major muscle hypertrophy-stimulating pathway induced by IGF-1, to depress muscle protein synthesis (McFarlane et al., 2006). Activation of muscle protein degradation by myostatin is thought to occur by increasing the expressions of two genes, atrogin-1 and muscle RING-finger 1 (MuRF1), which promote muscle protein breakdown primarily through the ubiquitin-proteasome proteolytic pathway (McFarlane et al., 2006; Satori et al., 2009). These findings clearly indicate that myostatin not only inhibits prenatal increase in muscle fiber number by suppressing myoblast proliferation and differentiation, but also inhibits postnatal increase in muscle fiber size through depressing muscle protein turnover. It, therefore, appears that blocking myostatin function may offer a strategy for enhancing muscle growth in agriculture animals as well as for treating muscular disorders in humans.

1.6. Bone formation

The formation of bone during the fetal stage occurs through two different processes, including intramembranous ossification and endochondral ossification. Flat bones (e.g. skull bones) are formed by intramembranous ossification while long bones (e.g. limb bones) and most of the rest of the bone in the body (e.g. spines) are formed by endochondral ossification. During intramembranous ossification, osteoblast progenitor cells within the mesoderm-originated mesenchyme directly differentiate toward osteoblasts, which secrete osteoid, mainly type 1 collagen, into extracellular matrix. Once minerals, mainly calcium, are deposited in the matrix,

bone is formed. However, during endochondral ossification, mesenchymal stem cells first differentiate into chondroblasts to form the cartilage model for the future bone, which then will be ossified by osteoblasts that are differentiated from the osteoprogenitor cells transported by the blood to the cartilage scaffold. Blood vessels also carry macrophages, which later form osteoclasts that are responsible for breaking down bone tissue, to the ossifying cartilage model. Although most part of the cartilage model will be replaced by bone after endochondral ossification, a cartilage plate called the growth plate is left in the epiphysis (the end) of the bone, and it continues to form new cartilage, which is continuously replaced by bone, resulting in continuous increase in length of the bone until maturity. Many molecules, such as Tumor necrosis factor-alpha (TNF α), Melanoma inhibitory activity (MIA) and bone morphogenetic proteins (BMPs), are involved in osteogenic or chondrogenic differentiation of mesenchymal stem cells during skeletogenesis, since all these factors have the ability to induce differentiation of cultured mesenchymal stem cells into osteoblasts or chondroblasts (Shea et al., 2003; Tscheudschilsuren et al., 2006; Hess et al., 2009; Steinert et al., 2009).

1.7. Bone and calcium metabolism

Bone serves as a reservoir for minerals, mainly calcium. About 99% of the calcium in the body is stored in bones. Calcium level in the blood must be controlled within a narrow range for maintaining normal physiological function. When intake of calcium is inadequate, the body will break down bone to release calcium to maintain the normal blood calcium level. When dietary calcium is adequate, the body will store calcium on bone by building new bone (before maturity) or by rebuilding the lost bone (after maturity). Hence, bone is a dynamic tissue that is remodeled throughout the whole life.

Calcium concentration in the blood is tightly regulated by several major hormones, including Vitamin D, parathyroid hormone (PTH) and calcitonin (Tordoss et al., 1998). The major form of Vitamin D in vertebrates is Vitamin D₃ (also called cholecalciferol or calciol), which is made in the skin when 7-dehydrocholesterol is exposed under ultraviolet light (Hume et al., 1927). After synthesis, Vitamin D₃ is carried by bloodstream to the liver, where it is converted into calcidiol (also known as calcifediol or 25-hydroxycholecalciferol, or 25-hydroxyvitamin D). Calcidiol then is converted in the kidney into calcitriol, the biologically active form of vitamin D. When blood calcium level is lower than the normal level, parathyroid hormone is secreted by the parathyroid glands to stimulate the conversion of Vitamin D into its active form, calcitriol, in the kidneys. Calcitriol acts to increase the absorption of dietary calcium from small intestine. Together with parathyroid hormone, calcitriol also stimulates the release of calcium from bone by enhancing the activity of bone resorption-responsible osteoclasts (Suda et al., 1995; Langman, 2000). In addition, parathyroid hormone and calcitriol works together to decrease the urinary excretion of calcium by increasing its reabsorption in the kidney. When blood calcium level is higher than the normal level, calcitonin, a hormone that counteracts parathyroid hormone, is secreted by the thyroid glands to reduce calcium levels in the blood (Copp and Cheney, 1962). The effects of calcitonin on regulating blood calcium level is through the inhibition of calcium absorption in the small intestine, the suppression of osteoclast activity in bones and the depression of reabsorption of calcium in the kidneys.

1.8. Regulation of bone growth

Bone growth involves establishment of skeletal elements and changes in bone size and bone mineral content. Although bone growth can be affected by embryonic establishment of skeletal elements, it is mostly determined by postnatal alteration in size and bone mineral content.

For the bones that are formed by intramembranous ossification, increase in size is achieved by new bone being laid down by the osteogenic layer. For most of the body bones, which are formed by endochondral ossification, increase in size is mainly decided by the chondrogenesis activity in their epiphyseal growth plates. For bone mineral content, it depends on the net balance between osteoblast-mediated mineral deposition and osteoclast-mediated mineral resorption. Therefore, postnatal bone growth involves three major cellular events, including chondroblast-determined increase of bone size, osteoblast-responsible bone building and osteoclast-mediated bone breakdown. In other word, bone growth is determined by the number and function of these three bone related cells. Bone morphogenetic proteins (BMPs) and their antagonists, such as follistatin and noggin, have been shown to play essential roles in bone growth by regulating osteoblastogenesis, osteoclastogenesis and chondrogenesis (Canalis et al., 2003; Canalis, 2009). Growth hormone-dependent IGF-1 also is very important for controlling bone mass during postnatal life through mediating osteoblast and osteoclast function (Canalis, 2009). The Wnt/ β -catenin pathway also plays a critical role in osteoblastogenesis as well as osteoclastogenesis (Canalis, 2009). In addition, a transcription factor, Runx2, is essential for intramembranous and endochondral bone formation, since it is required for osteoblast formation and chondrocyte differentiation (Ducy et al., 1997; Komori et al., 1997; Enomoto et al., 2000).

1.9. GDF11 and bone growth

A number of growth factors regulate bone growth. One of the transforming growth factor- β (TGF- β) superfamily members, growth differentiation factor 11 (GDF11) which is also called bone morphogenetic protein 11 (BMP11), is a newly identified BMP member that has been shown to play essential roles in skeletal patterning and formation. GDF11 share a remarkable high homology (90%) with myostatin in amino acid sequence (Gamer et al., 1999; Nakashima et

al., 1991). Knockout of GDF11 showed that GDF11 plays a very critical role in regulating the anterior/posterior axial skeleton patterning. Homozygous GDF11-deficient mice exhibited dramatic transformation of axial skeleton wherein the identities of caudal vertebrae were converted into those of more cranial vertebrae (McPherron et al., 1999). GDF11 was believed to signal through Hox genes, a group of transcription factors that function to specify the identities of vertebrae, to regulate axial skeleton formation (McPherron et al., 1999). GDF-11 also was demonstrated to play an important role in the formation and development of limb skeleton, as implantation of GDF11 beads in the early wing bud caused dramatic shortening of forelimb in chicken embryos (Gamer et al., 2001). The significant truncation of limb skeleton seen in GDF11-treated chicken embryos was thought to be mainly caused by the strong negative effect of GDF11 on chondrogenesis (Gamer et al., 2001). Targeted disruption of GDF11 in the genetic background lacking myostatin, which is redundant to GDF11 in regulating skeletal formation, further showed that GDF11 regulates limb skeleton formation as well as axial vertebral formation (McPherron et al., 2009). In addition, blocking GDF-11 signaling by deletion of GDF11 receptors (Oh and Li, 1997; Oh et al., 2002 and Andersson et al., 2006) or inactivation of the proteinase for processing GDF11 precursor protein (Essalmani et al., 2008) caused similar defects in axial skeletal patterning observed in GDF11-null mice.

All these results strongly indicate that GDF11 is necessary for normal skeletal formation, and ligands that regulate GDF11 signaling may also be important for bone growth.

1.10. Regulation of the activities of myostatin and GDF11 by their own propeptides

Some of the TGF- β superfamily members, such as TGF- β 1, 2 and 3, are synthesized as precursors containing N-terminal propeptides that can form a latent complex with their own C-

terminal mature proteins to inactivate their activities, following the proteolysis by furin-like convertases (Böttlinger et al., 1996). Like the propeptides of TGF- β 1, 2 and 3, myostatin propeptide, which is generated from the N-terminal propeptide of the myostatin precursor after proteolytic processing, also was shown to form a latent complex with mature myostatin both in vitro and in vivo (Lee and McPherron, 2001; Thies et al., 2001; Zimmers et al., 2002). In addition, the mouse myostatin propeptide was demonstrated to enhance muscle growth in vivo by suppressing myostatin function (Lee and McPherron, 2001; Yang et al., 2001), and its own activity is inhibited by BMP-1/TLD-like metalloproteinases (Pirrottin et al., 2005; Wolfman et al., 2003). Similarly, the GDF11 propeptide, which is the N-terminal propeptide cleaved from the GDF11 precursor, also was shown to depress GDF11 activity in vitro by forming a latent complex with it (Ge et al., 2005).

1.11. Hypotheses and research objectives

Myostatin and GDF11 are critical for muscle and bone growth, respectively. Mouse myostatin propeptide has been shown to depress myostatin activity in vitro and enhance muscle growth in vivo. However, whether the myostatin propeptide also acts to promote muscle growth by antagonizing myostatin activity in pigs remains unknown. Although GDF11 propeptide has been shown to depress GDF11 activity in vitro (Ge et al., 2005), its in vivo effect on bone growth has not yet been reported. Our hypotheses are: (1) the pig myostatin propeptide will promote muscle growth by suppressing myostatin function; (2) the GDF11 propeptide also regulates bone growth by depressing GDF11 function. In order to test these hypotheses, the present project has two research objectives: (1) To investigate the effects of a BMP-1/TLD-like metalloproteinases-resistant pig myostatin propeptide (a mutated pig myostatin propeptide) on muscle growth in mice, (2) To generate transgenic mouse over-expressing GDF11 propeptide in

skeleton as a model system to investigate the physiological function of GDF11 propeptide in bone growth. To achieve objective 1, I produced wild-type and mutated porcine myostatin propeptides in insect cells and compared their abilities to block myostatin activity in vitro, followed by injecting the mutated porcine myostatin propeptide into mice to study its in vivo effects on muscle growth. To accomplish objective 2, I generated transgenic mice over-expressing GDF11 propeptide under the control of a bone-specific promoter, and used these transgenic mice as models to study the function of GDF11 propeptide in regulating bone growth by analyzing their skeletal phenotype.

CHAPTER 2

SUPPRESSION OF MYOSTATIN BY A MUTATED PIG MYOSTATIN PROPEPTIDE

2.1. Abstract

Growth differentiation factor 8 (GDF8), also referred to as myostatin, is a dominant inhibitor of skeletal muscle growth. Myostatin propeptide is a ligand that has been shown to enhance muscle growth by suppressing myostatin function. Recently, it has been further demonstrated that a mouse myostatin propeptide that was mutated at the cleavage site of the BMP-1/TLD-like metalloproteinases was more effective in promoting muscle growth than the wild-type mouse myostatin propeptide. I hypothesize that a BMP-1/TLD-like metalloproteinases-resistant pig myostatin propeptide is also more effective in blocking myostatin activity than its wild-type counterpart and administration of the BMP-1/TLD-like metalloproteinases-resistant pig myostatin propeptide into animals can enhance muscle growth. In this study, I produced the wild-type form and a mutated form (BMP-1/TLD-like metalloproteinases-resistant) of porcine myostatin propeptides in insect cells. *In vitro* reporter assays showed that both wild-type and mutated propeptides have a similar capacity in depressing myostatin activity in 6h co-incubation in A204 cells. However, the mutated propeptide appeared more effective in blocking myostatin activity than wild-type propeptide when the *in vitro* co-incubation time was increased to 24h or 48h. Administration of the mutated propeptide to neonatal mice resulted in an increase of growth performance by 11–15% from the age of 25 to 57 days ($P < 0.05$). The major skeletal muscles of mice that were injected with mutated propeptide were 13.5–24.8% heavier than the controls ($P < 0.05$) as a result of muscle fiber hypertrophy. In conclusion, mutating the cleavage site of BMP-1/TLD-like metalloproteinases in pig myostatin

propeptide increased its effect on suppressing myostatin activity. Administration of the BMP-1/TLD-like metalloproteinases-resistant pig myostatin propeptide to mice significantly enhanced muscle growth, suggesting it may have application for promoting muscle growth in pigs.

2.2. Introduction

Growth differentiation factor 8 (GDF8), also known as myostatin, is a significant inhibitor for muscle growth. In order to develop strategies for promoting muscle growth by blocking myostatin function, many studies have been done to investigate the regulation of myostatin signaling pathway.

Like some other members of the TGF- β superfamily, myostatin is initially translated as a precursor consisting of the N-terminal signal peptide, the myostatin propeptide and the C-terminal myostatin mature peptide with the conserved cysteine residues found in all TGF- β members (McPherron and Lee, 1997 and Lee, 2004). After translation, myostatin forms a dimer by linking two precursor molecules at the C-terminal mature peptide with a disulfide bond (Lee, 2004). Following the removal of the signal peptide, the proprotein convertases of the furin family is believed to cleave the myostatin precursor dimer at a conserved tetrabasic site (RXRR) to generate the myostatin propeptide and the C-terminal mature peptide dimer (Lee, 2004). After the proteolytic processing of the precursor, myostatin is secreted as an inactive latent complex of a mature peptide dimer bound by the propeptide or other myostatin-binding proteins, such as follistatin and the follistatin related protein (Thies et al., 2001; Hill et al., 200; Lee, 2004 and Lee, 2007). In the circulation, one mechanism for activating myostatin from the latent complex appears to be through the cleavage of the myostatin propeptide in the latent complex by bone morphogenetic proteins-1/tolloid (BMP-1/TLD)-like metalloproteinases (Wolfman et al., 2003;

Lee, 2008). Following the release from the latent complex, the myostatin mature peptide dimer, binds to myostatin receptors, such as activin type II receptors -A and -B, to induce the downstream signaling pathway for regulation of muscle growth (Lee and McPherron, 2001 and Rebbapragada et al., 2003).

Based on the signaling pathway of myostatin, several different molecular approaches have been employed to block its function. Muscle-specific transgenic over-expression of different myostatin antagonists, including myostatin propeptide (Lee and McPherron, 2001; Yang et al., 2001 and Pirottin et al., 2005), follistatin (Lee and McPherron, 2001), the follistatin related protein (Lee, 2007) and mutant activin type II receptor-B (Lee and McPherron, 2001), have been demonstrated to cause dramatic increase of muscle mass in mice. Direct administration of recombinant mutant activin type II receptor-B to normal mice (Lee et al., 2005) also significantly promoted muscle growth. Furthermore, injections of anti-myostatin antibodies have also been indicated to increase muscle weight in chickens (Kim et al., 2006 and 2007), normal mice (Whittemore et al., 2003) or mice with muscular dystrophy (Bogdanovich et al., 2002). Among these investigated myostatin antagonists, I am most interested in myostatin propeptide. Our previous study already showed that transgenic over-expression of this ligand specifically in muscle tissues of mice resulted in 17-30% increase of body weight and 22-44% increase of muscle mass while the fat mass was significantly decreased (Yang et al., 2001). The dramatic increase of muscularity displayed in the transgenic mice over-expressing myostatin propeptide suggests that direct administration of recombinant myostatin propeptide to animals may also promote muscle growth. However, recent studies indicated that a myostatin propeptide which was mutated at the cleavage site of the BMP-1/TLD-like metalloproteinases was much more effective in promoting muscle growth than a wild-type myostatin propeptide, because injection

of the mutated myostatin propeptide into adult normal mice caused approximately 20% increase of muscle mass while the wild-type myostatin propeptide has little effect on muscle growth of the injected mice (Wolfman et al., 2003). This suggests that an introduced mutation to myostatin propeptide at the cleavage site of BMP-1/TLD-like metalloproteinases enhances its effect on suppressing myostatin activity by increasing the stability of myostatin latent complex.

The pig is an important meat animal in the USA as well as many Asian countries. Our laboratory is interested in applying the myostatin propeptide to improve muscle growth in pigs. However, only the mouse myostatin propeptide has been investigated. It is not known whether a BMP-1/TLD-like metalloproteinases-resistant pig myostatin propeptide has a stronger effect on blocking myostatin activity than the wild-type pig myostatin propeptide. Whether a mutated form of pig myostatin propeptide has applications for enhancing muscle growth in animals is also unknown. To answer these two questions, I produced wild-type and mutated pig myostatin propeptide from an insect cell expression system and then compare their abilities to suppress myostatin activity *in vitro* followed by injecting the mutated form of pig myostatin propeptide into neonatal mice to study its effects on muscle growth.

2.3. Materials and methods

2.3.1. Plasmid construction and preparation

Myostatin propeptide cDNA (encoding for pig myostatin amino acid residue 1-265, Genbank accession number AF019623) was amplified from plasmid pMLC-mstnpro (Wu et al., 2008) and cloned into the multiple cloning site (between the Nco 1 and Xho 1 sites) upstream of a His.tag in the insect cell expression plasmid pIEX-5 (Novagen, Darmstadt, Germany) to generate the recombinant plasmid pIEX-5-Ppro. A green fluorescent protein (GFP) gene also

was cloned into the same site of pIEX-5 to generate the control plasmid pIEX-5-GFP. A nucleotide point mutation (a224c), which causes a corresponding residue change of aspartate (D) to alanine (A), was introduced into the myostatin propeptide gene in the pIEX-5-Ppro plasmid by using the Phusion Site-Directed Mutagenesis Kit (Finnzymes, Espoo, Finland). The accuracies of the reading frames of plasmid pIEX-5-Ppro, pIEX-5-Pmpro and pIEX-5-GFP were confirmed by sequencing and restriction enzyme digestions. Plasmids were transformed into DH5 α competent cells (Invitrogen, Carlsbad, CA) and propagated at 37 °C, 250 rpm for 12-16 hours and purified with the Endotoxin-free Plasmid Midi Kit (Qiagen, Valencia CA) according to the manufacturer's instructions. Purified plasmids were diluted in TE buffer to a final concentration of 1 $\mu\text{g}/\mu\text{l}$.

2.3.2. Cell culture and transfection

Wild-type and mutated propeptides were produced using the InsectDirect System (Novagen, Darmstadt, Germany). Sf9 insect cells were cultured in BacVector Medium (Novagen) at 28°C as recommended by the manufacturer. To perform transient transfection, 20 μg of plasmid was mixed with 100 μl of Insect GeneJuice Transfection Reagent (Novagen, Darmstadt, Germany) in 2 ml of medium and incubated at room temperature for 15 min and then added to 75 cm^2 cell culture flask containing about 10×10^6 cells (~75% confluency) and 8 ml of medium. The transfected cells were incubated at 28°C until harvested.

2.3.3. Protein expression and purification

For time-course analysis, at 24 h, 48 h and 72 h after transfection with pIEX-5-Pmpro plasmid, 30 μl of medium (medium protein) was collected from flasks and then subjected to SDS-PAGE analysis. Total protein (cell protein+medium protein) was harvested by adding 500

μ l of Insect PopCulture Reagent (Novagen, Darmstadt, Germany) and 100 U of Benzonase Nuclease to each flask and incubating at room temperature with gentle shaking for 20 min. A volume of 30 μ l of total protein was used for SDS-PAGE. For large-scale propeptide production, total protein was harvested at 48 h after plasmid transfection as described above. Recombinant propeptide was purified from total protein with Insect RoboPop Ni-NTA His.Bind Purification Kit (Novagen, Darmstadt, Germany) following the manufacturer's recommendation. Purified protein was then concentrated and desalted by Amicon® Ultra-4 Centrifugal Filter Units (Millipore). The concentration of protein was determined by BCA Protein Assay kit (Pierce Biotechnology). 1 μ g of purified protein was subjected to SDS-PAGE followed by Western blot.

2.3.4. SDS-PAGE and Western Blotting analyses

SDS-PAGE was performed according to a method used by Laemmli (1970) . Samples were mixed with loading buffer in the presence of (reducing conditions) or absence of 1.5% β -mercaptoethanol (non-reducing conditions) and separated in 12% SDS-polyacrylamide mini gels. Proteins in the gels were visualized by silver staining. For Western blotting, proteins were transferred onto a PVDF membrane after SDS-PAGE electrophoresis. The membranes were incubated with mouse monoclonal anti-His.tag antibody (Novagen, Darmstadt, Germany) or goat polyclonal anti-myostatin propeptide antibody (Santa Cruz Biotechnology, Santa Cruz, CA. Cat. #: SC-6885) and then with goat anti-mouse IgG-HRP secondary antibodies or rabbit anti-goat IgG-HRP secondary antibodies (Santa Cruz Biotechnology, Santa Cruz, CA), followed by incubation with Visualizer™ chemiluminescent detection reagents (Upstate biotech, Lake Placid, NY). Western blot signals on the membrane were exposed to films in a dark room and then exposed films were processed through a film developer to develop blot images.

2.3.5. pGL3-(CAGA)12-luciferase reporter assay in A204 rhabdomyosarcoma cells

The capability of myostatin propeptide to inhibit myostatin activity *in vitro* was measured by using the pGL3-(CAGA)12-firefly luciferase reporter assay in A204 rhabdomyosarcoma cells (ATCC, HTB-82) as described by Thies et al. (2001). Briefly, A204 cells were seeded in a 96 well plate at 40,000 cells/200 μ l/well and grown in DMEM containing 10% fetal bovine serum, 10,000 U/ml of penicillin and 10 mg/ml of streptomycin at 37°C with 5% CO². After 24 h, cells were transiently transfected with 0.1 μ g of pGL3-(CAGA)12 plasmid which carried a firefly luciferase gene under the control of a myostatin-activated promoter, the (CAGA)12 box (Dennler et al., 1998), by using FuGENE 6 Transfection Reagent (Roche, Mannheim, Germany). Each well was also transfected with 0.01 μ g of pRL-TK plasmid (Promega, Madison, WI), which carried a renilla luciferase gene and was used as a control plasmid to calibrate the transfection efficiency. At 24 h after transfection, medium was replaced with serum-free medium, and further incubated for 9 h. Twenty ng/ml of mouse myostatin (R&D Systems, Minneapolis, MN) and various concentrations of myostatin propeptide were added to each well, and incubated for another 6 h. At the end of incubation, luciferase activity, which represents myostatin activity, were measured by Veritas microplate luminometer (Turner Biosystems, Sunnyvale, CA) using Dual Luciferase Assay System (Promega, Madison, WI) according to the manual provided by the manufacturer. The luciferase activity of the wells that were incubated only with myostatin was defined as 100%. For different co-incubation time analysis, cells were prepared as described above. After the cells were incubated with serum-free medium for 9 hrs, 20 ng/ml of mouse myostatin with 100ng/ml of mutated or native propeptide were added to the wells. Luciferase activities were measured after 6, 24 and 48 h co-incubation. The luciferase activity of the wells that were only added with myostatin was defined as 100%.

2.3.6. Administration of propeptide to neonatal mice

Animal use and care for this study were approved by the Institutional Animal Care and Use Committee of University of Hawaii. Mice were housed in cages; room temperature was maintained at 22°C and 12-h light/dark cycle. Mice were given free access to a chow diet (10% kcal fat, ME3.85 kcal/g). Five adult B6SJL females were mated with a same B6SJL male to produce 5 litters of half sibling pups (7-8 pups/litter). Three neonatal mice (without sex identifications) were randomly chosen from each litter and given an intraperitoneal injection of propeptide at a dose of 10mg/kg of body weight at the age of 11 and 18 days. The remainders of the animals in each litter were injected with the same volume of PBS to be used as controls. Mice were weaned at the age of 21 days, separated individually and raised under the same conditions as above. At the age of 57 days, mice were euthanized by CO² and subjected to muscle weight and histology analysis. Carcass and muscle mass were determined as described (Yang and Zhao, 2006). Growth data were collected by weighting the mice once a week, starting from the first injection.

2.3.7. Determination of muscle fiber size

The longissimus dorsi muscles were removed within 5 minutes after euthanizing the animals. Samples were fixed in 4% of paraformaldehyde, embedded in paraffin. Muscle sections were then cut by microtome, mounted on glass slides and stained with hematoxylin and eosin. The stained sections were observed at 100× under a microscope. Four random images at different locations within one section were captured with a camera connected to the microscope. Within each of the captured images, four different spots (each spot contains multiple adjacent muscle fibers) were randomly selected and the area of each spot was measured with the Quantity One

software (Bio-Rad) and the total fiber number within each spot was counted. The average muscle fiber cross section area for each animal was calculated by dividing the sum of area of randomly selected 16 spots from four images by the sum of fiber numbers within corresponding 16 spots.

2.3.8. Statistical analysis

Data were analyzed by SAS 9.2 program (SAS Institute, Cary, NC), and the two samples t-test for means program was used for mean comparisons in Table 2.1, Figure 2.4, Figure 2.5 and Figure 2.6. Data are present as mean \pm standard error of mean (SEM) or mean \pm standard deviation (SD). Significant difference of means between two different groups was determined at $P < 0.05$ (*) or $P < 0.01$ (**).

2.4. Results

2.4.1. Production of wild-type and mutated porcine myostatin propeptides from insect cells

The transfection efficiency of the pig myostatin propeptide expression plasmids to insect cells was monitored by transfecting control plasmid pIEX-5-GFP into insect cells. The transfection efficiency was estimated to be over 50% (Figure 2.1). Expression of recombinant propeptide was detected in total protein (cell protein + medium protein) and only in medium protein in Sf9 insect cell culture at different time points after transfection, by SDS-PAGE (Figure. 2.2A) and Western blot (Figure. 2.2B). The recombinant proteins in both total protein and medium protein were reactive with anti-His.taq antibody and the size of recombinant proteins were matched with the molecular weight (34.3 kDa) of recombinant pig myostatin propeptide (Figure. 2.2B). No protein signal was detected from non-transfected insect cells by using the same antibody (anti-His.taq antibody) and conditions during Western blot analysis (data not shown). The amount of recombinant propeptide in total protein of insect cell culture

appeared higher than that only in the medium, regardless of the collection time of 24, 48, or 72 h post-transfection (see Figure 2.2B). This suggests that purification of the recombinant protein from total protein instead of medium will obtain more recombinant propeptides. The yield of recombinant propeptide in total protein was higher at 48 h post-transfection than the other times (Figure 2.2B), suggesting that harvesting insect cells at 48 h post-transfection for protein purification provides more recombinant propeptides. Based on these results, both wild-type and mutated pig myostatin propeptides were expressed and purified from sf9 insect cells. The purities and identities of purified recombinant propeptides were further examined by SDS-PAGE and Western blot under reducing or nonreducing conditions. The 34.3 kDa proteins band present in the SDS-PAGE and Western blotting analysis with anti-his.tag antibody were confirmed as recombinant myostatin propeptide by Western blot with anti-myostatin propeptide antibody (Figure 2.2C). In Western blotting analysis under reducing conditions, both the wild-type and mutated myostatin propeptides were present as monomers (34.3 kDa, Figure 2.2C). However, the monomeric pig myostatin propeptide and a larger protein (\approx 160 kDa) were present in Western blotting analysis under nonreducing conditions (Figure 2.2D). Since this high molecular-weight protein was reactive to anti-his.tag antibody, it is most likely a misfolded myostatin propeptide that resulted from propeptide aggregation under nonreducing conditions.

2.4.2. Effects of wild-type and mutated propeptide on blocking myostatin activity *in vitro*

Both the wild-type and mutated pig myostatin propeptide showed similar capabilities in blocking myostatin activity in 6h co-incubation in A204 cells (Figure 2.3). The activity of myostatin (20 ng/ml) started to decrease when the concentration of co-incubated propeptide reached 50 ng/ml (Figure 2.3). More than 80% of myostatin activity was blocked by 100 ng/ml of propeptide while myostatin activity was almost completely suppressed by 500 ng/ml or a higher

concentration of propeptide (Figure 2.3). To test the abilities of both wild-type and mutated propeptide to block myostatin activity in a longer incubation time, propeptide (100ng/ml) and myostatin (20ng/ml) were co-incubated in the A204 cells for 24h and 48 h. The abilities of both wild-type and mutated propeptides to block myostatin activity decreased at 24 and 48 h co-incubation, compared to that at 6 h co-incubation (Figure 2.4). However, the capability of wild-type propeptide to suppress myostatin activity decreased faster than the mutated propeptide during 24h and 48 h of co-incubation (Figure 2.4). After 24 h co-incubation, the wild-type propeptide only depressed approximately 65%, but the mutated propeptide suppressed more than 75% of myostatin activity. After 48h co-incubation, the wild-type propeptide inhibited less than 30% while the mutated propeptide blocked approximately 60% of myostatin activity (Figure 2.4).

2.4.3. Administration of mutated propeptide to neonatal mice significantly increased muscle growth

Based on the results from the *in vitro* assays, we believed that the mutated propeptide will show positive effects on *in vivo* muscle growth. Given the high cost for production of recombinant proteins, animal experiments were only performed for the mutated porcine myostatin propeptide. The effect of mutant propeptide on muscle growth was rapid and significant. Injection of mutated propeptide caused a significant increase in body weight at as early as 1 week after the first injection in female mice (Figure 2.5B), and 1 week after the second injection in male mice (Figure 2.5A), in comparison with their controls. After the second injection, male mice injected with mutated propeptide were 12–15% heavier than their controls ($P<0.05$) from the age of 25 to 57 days (Figure 2.5A), whereas female mice injected with the propeptide were 11–15% heavier than their controls ($P<0.05$) from the age of 25 to 57 days

(Figure 2.5B). The effect of the mutated propeptide on muscle growth was maintained for at least 1 month (from the age of 25 to 57 days).

At the age of 57 days, animals were sacrificed to measure the weight of carcass and major skeletal muscles. The muscle weights of mice injected with propeptide were significantly increased in comparison with the mice injected with PBS. As shown in Table 2.1, injection of mutated propeptide significantly increased carcass weight by 19.5% and 17.7% in males and females, respectively. In regard to individual muscles, the injection also led to a significant increase of 13.5–24.8% in the major skeletal muscles in both males and females except that the increase in pectoralis, longissimus dorsi, and gastrocnemius muscle weight in female was not statistically significant (Table 2.1).

Analysis of fiber size of longissimus dorsi muscle from male mice injected with propeptide showed that the average cross-section area of muscle fiber was significantly increased by 25% in comparison with the control group ($1,826.1 \mu\text{m}^2$ vs. $1,466.1 \mu\text{m}^2$, $n=4$ in both groups, see Figure 2.6A-C).

2.5. Discussion and conclusions

The pGL3-(CAGA)₁₂-firefly luciferase reporter assay in human A204 rhabdomyosarcoma cells has been used for analyzing myostatin activity (Thies et al., 2001). In this study, the mutant form of porcine myostatin propeptides showed a similar ability to block myostatin activity with the wild-type form in 6h co-incubation in A204 cells (Figure 2.3). This result indicates that the aspartate to alanine mutation at the proteolytic cleavage site of BMP-1/TLD-like metalloproteinases in porcine myostatin propeptide did not impair the binding activity of the propeptide to myostatin. In addition, when co-incubated in A204 cells for 6h, 90% inhibition of

20 ng/ml (2 pM) myostatin activity occurred at around 250 ng/mL(7.5 pM) of recombinant pig myostatin propeptide (Figure 2.3). This result suggest that less than a four-fold ratio of propeptide-to-myostatin is sufficient to inhibit most of myostatin activity, which is comparable with our earlier estimate that approximately three-fold of propeptide was sufficient to suppress most myostatin activity (Bobbili et al., 2008). Although the mutant and wild-type forms of porcine myostatin propeptides were equally effective in suppressing myostatin activity in 6h co-incubation assay, the mutated porcine myostatin propeptides showed a much stronger effect on depressing myostatin activity than the wild-type counterpart when the co-incubation time was increased to 24h or 48h. These results indicate that the mutant form of pig myostatin propeptide has enhanced resistance to the proteolysis by BMP-1/TLD-like metalloproteinases or other unknown proteinases, hence increase its ability to maintain the myostatin mature peptide in the latent complex.

It is well recognized that neonatal animals have a high rate of protein synthesis, particularly in skeletal muscle. A high muscle protein synthesis rate, which usually determines the whole body growth rate, is mostly driven by the high sensitivity of response to hormonal stimuli during the neonatal period (Davis et al., 2002). Myostatin protein abundance has been shown to be negatively correlated with muscle protein synthesis rate in neonatal rat and administration of a myostatin inhibitor, follistatin, to neonatal rats increased muscle protein synthesis rate by approximately 20% (Suryawan et al., 2006). To investigate the in vivo effects of the BMP-1/TLD-like metalloproteinase-resistant pig myostatin propeptide on muscle growth, we used neonatal mice for the injection study. The results showed that only two injections of the mutated propeptide at the neonatal stage was sufficient to stimulate a 11-15% increase in body weight during a period of approximately one month after the second injection (Figure 2.5). This suggests

that promotion of muscle growth by down-regulating myostatin activity is more effective when administered during the neonatal stage than the adult stage, since multiple continuous injections of myostatin antagonists were usually required for enhancing muscle growth in adult animals (Wolfman et al., 2003; Lee et al, 2005). In this study, growth of animals injected with mutated propeptide appears slowed from the age of 53-57 days (Figure 2.5), suggesting the injected propeptide started to lose its effect on muscle growth. Continuous injections or a higher dose of the propeptide may be needed for sustained growth enhancement.

In mammals, muscle fiber number is determined during embryonic development (Luff and Goldspink, 1970; Wegner et al., 2000). Postnatal muscle growth primarily results from muscle fiber enlargement. Given that the overall volume of muscle fiber is roughly proportional to the cross-section area of the fiber, the observed enlargement of muscle fiber size (25%, see Figure 2.6C) in mice injected with mutated propeptide would cause a similar magnitude of increase in muscle fiber volume, which seems was fully responsible for the overall increase in skeletal muscle mass (13.5–24.8%, see Table 2.1). Therefore, the muscle histology results of this study confirmed that increase of muscle mass in mice administered with mutated pig myostatin propeptide mainly resulted from muscle fiber hypertrophy.

Since the identification of myostatin in 1997, several approaches have been developed to depress myostatin activity for enhancing muscle growth or reversing muscle loss. For example, direct injection of myostatin antibody (Bogdanovich et al., 2002; Whittemore et al., 2003), myostatin propeptide (Wolfman et al., 2003; Bogdanovich et al., 2005), follistatin (Suryawan et al., 2006), activin type II receptors B (Lee et al., 2005) or adeno-associated virus particles carrying myostatin propeptide (Bartoli et al., 2007) or follistatin (Haidet et al., 2008), have been tested in wild-type or muscular dystrophic animal models. All of these approaches appear useful

and practical in blocking myostatin for building muscle mass even though some methods need continuous multiple injections and may exhibit potential immune or viral responses. However, since it is experimentally challenging to enhance muscle growth in large-size animals and humans by recombinant protein or gene therapy approaches, none of these approaches, so far have been tested in large animals or human subjects. Their effects on muscle growth or prevention of muscle wasting in a large animal or human body are not known. In this study, BMP-1/TLD-like metalloproteinase-resistant porcine myostatin propeptide was produced and tested for its effect on muscle growth in mice. The data obtained from this study will help to direct future studies that aim to investigate the effect of the mutated pig myostatin propeptide on muscle growth in large animals, such as pig.

In conclusion, the BMP-1/TLD-like metalloproteinase-resistant porcine myostatin propeptide showed a similar activity with its wild-type counterpart in blocking myostatin activity after 6h co-incubation in A204 cell, but the former displayed a much stronger activity than the later in suppressing myostatin activity when the co-incubation time was increased to 24h or 48h. Administration of the mutated propeptide to neonatal mice significantly increased skeletal muscle growth, although we cannot exclude the possibility that the wild-type propeptide may have a similar *in vivo* effect on muscle growth. Enhanced muscle growth by twice injection of the mutated propeptide at neonatal stages lasted for about one month after the injections, and primarily resulted from muscle fiber hypertrophy. These results suggest that depression of myostatin activity by BMP-1/TLD proteinase-resistant porcine myostatin propeptide can be an effective way to promote muscle growth. The BMP-1/TLD proteinase-resistant porcine myostatin propeptide may have potential applications to boost muscle growth in pigs.

Table 2.1 Muscle weights of mice injected with mutated pig myostatin propeptide or PBS[#]

Muscles	Males			Females		
	PBS injection (n=16)	Propeptide injection (n=9)	Increase %	PBS injection (n=7)	Propeptide injection (n=6)	Increase %
Carcass	7,801±93	9,321±157**	19.5	6,217±122	7,318±63**	17.7
Longissimus dorsi	190±9	229±16*	20.5	137±11	158±12	15.3
Semitendinosus	118±4	139±5**	17.6	94±3	112±5*	18.4
Pectoralis	115±4	141±5**	22.7	74±4	87±6	17.5
Gastrocnemius	111±4	139±5**	24.8	101±5	115±8	13.9
Triceps	82±3	102±7**	23.9	70±3	85±5*	21.4
Tibialis	74±3	84±4*	13.5	59±3	70±4*	19.5

[#]Carcass and muscles were weighed in mg. Means ± SEM were presented, and the means between PBS inject group and propeptide injection group differ at P<0.05 (*) and P<0.01(**).

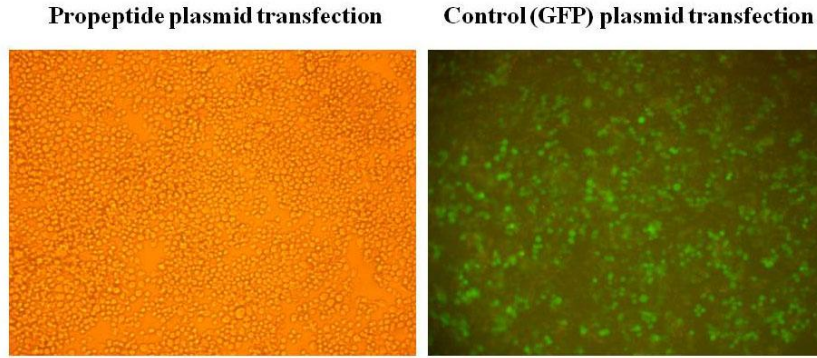


Figure 2.1 Transfection efficiency of recombinant protein expression plasmid in sf9 insect cells. Left panel shows the sf9 insect cells at 24h after transfecting with the insect cell expression plasmid pIEX-5-Pmpro carrying the mutated pig myostatin propeptide gene. Right panel shows the sf9 insect cells at 24h after transfecting with the insect cell expression plasmid pIEX-5-GFP carrying the green fluorescent protein (GFP) gene.

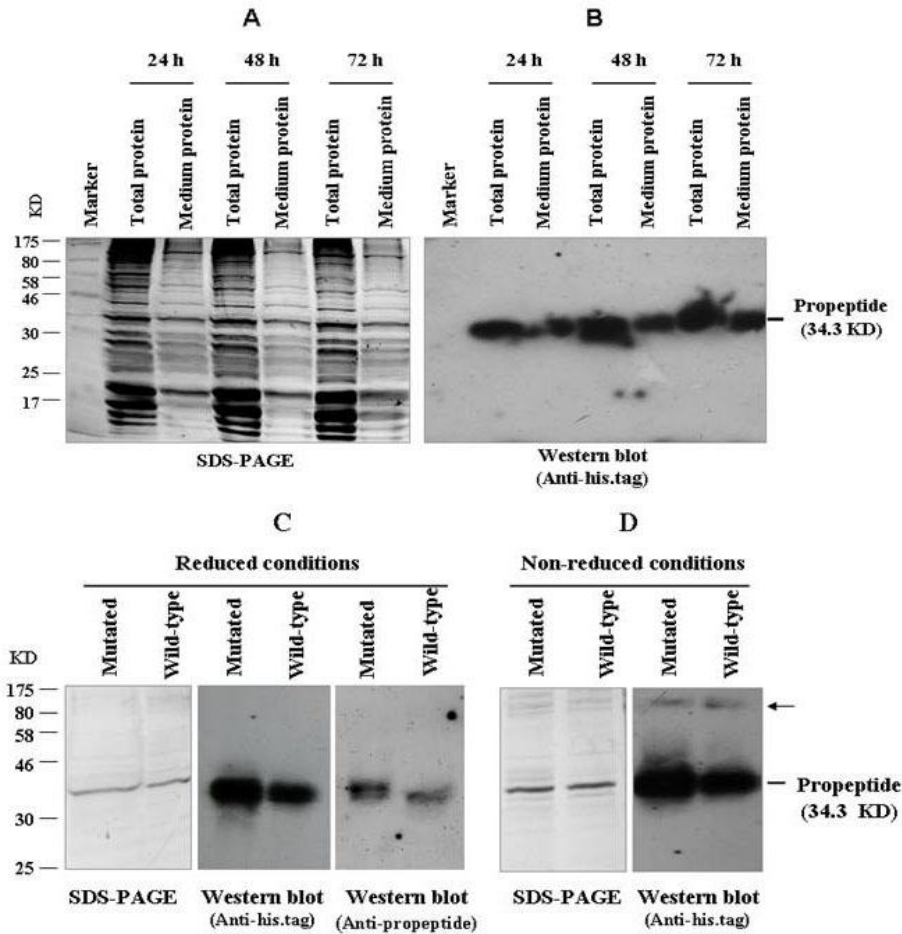


Figure 2.2 Production of wild-type and mutated porcine myostatin propeptide in insect cells. **A:** Total protein (cell protein + medium protein) and medium protein harvested at different times after the transfection were analyzed by SDS-PAGE. **B:** The same samples in subpart A were analyzed by Western blot with anti-his.tag primary antibody under reducing conditions. **C and D:** SDS-PAGE and Western blot with anti-his.tag or anti-myostatin propeptide primary antibodies were performed on the purified recombinant protein under reducing conditions or non-reduced conditions. The single bands indicated by the 34.3 KD in subpart B, C and D were presumably the mutated or wild-type pig myostatin propeptide. The band that is indicated by the right upper arrow in subpart D most likely represents misfolded propeptide under non-reduced conditions.

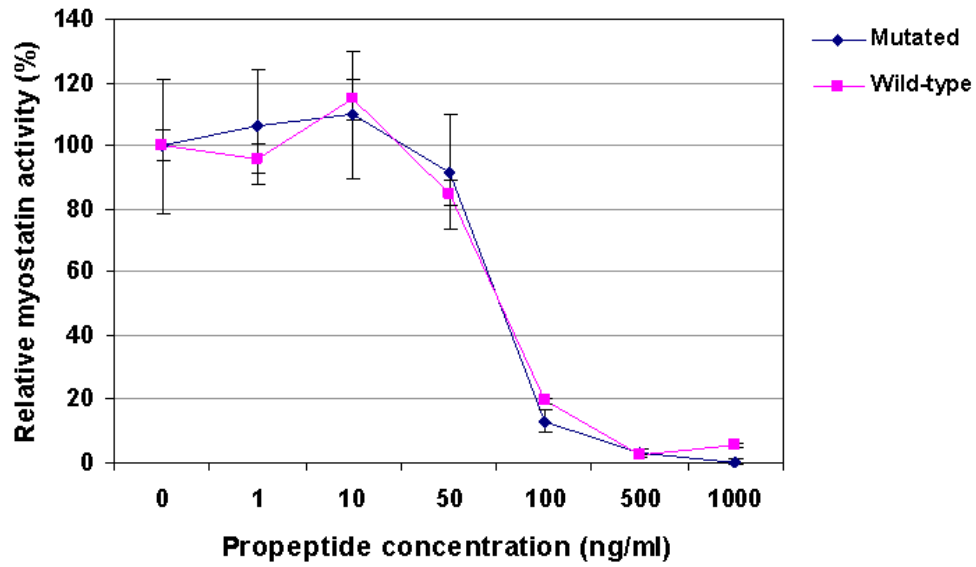


Figure 2.3 Inhibition of myostatin activity (20ng/ml) by different concentrations of wild-type or mutated pig myostatin propeptide after 6h co-incubation in A204 cells. n=6 in each concentration of wild-type or mutated propeptide, data are present as mean \pm SD.

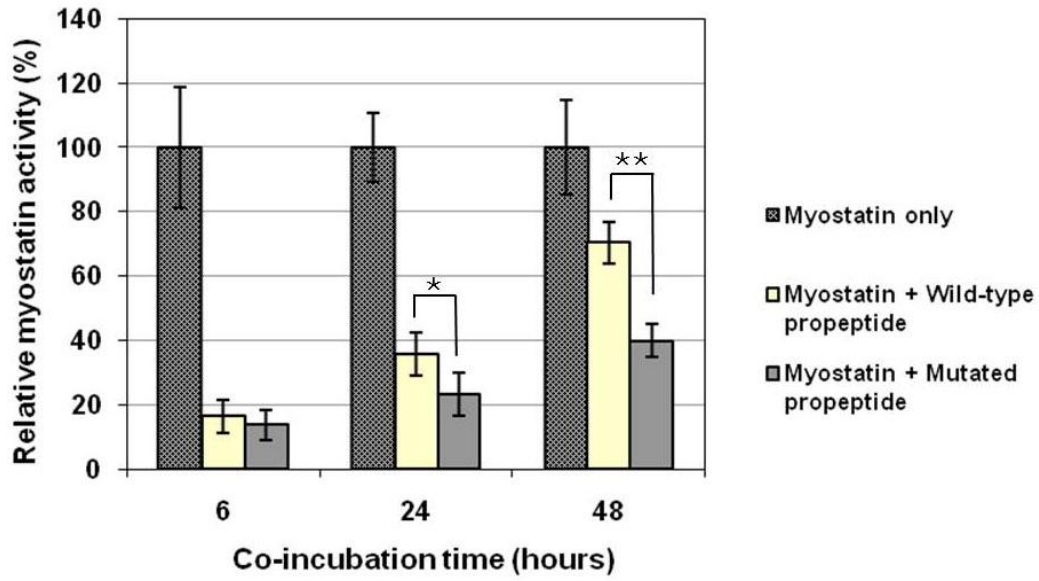


Figure 2.4 Inhibition of 20ng/ml of myostatin by 100ng/ml of wild-type or mutated pig myostatin propeptide after 6h, 24h and 48h co-incubation in A204 cells. n=6 in each co-incubation time, data are present as mean \pm SD. Means between two groups (myostatin + wild-type propeptide and myostatin + mutated propeptide) at each co-incubation time differ at $P < 0.05$ (*) and $P < 0.01$ (**).

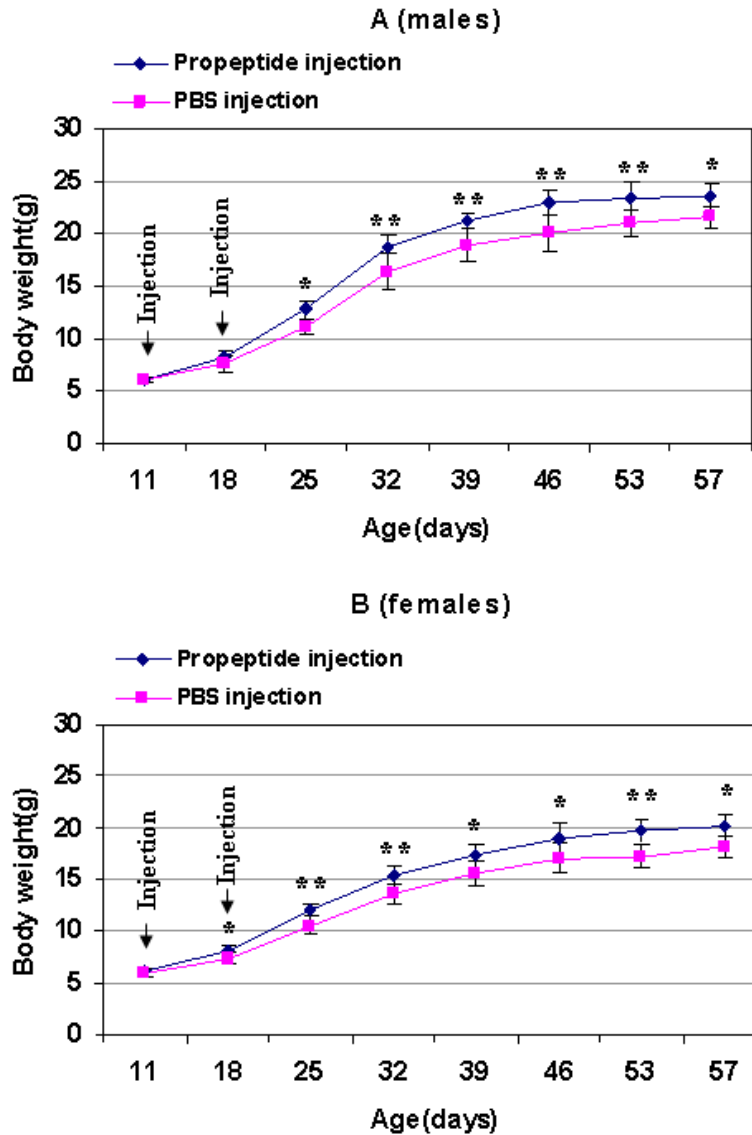


Figure 2.5 Growth curves of mice after injection with mutated pig myostatin propeptide or PBS. The growth curves of male mice after twice injections with mutated pig myostatin propeptide (n=9) or PBS (n=16) are shown in **A** while the growth curves of female mice after twice injections with mutated pig myostatin propeptide (n=6) or PBS (n=7) are shown in **B**. Data are present as mean \pm SD. Means between propeptide injection group and PBS injection group at each age differ at $P < 0.05$ (*) and $P < 0.01$ (**).

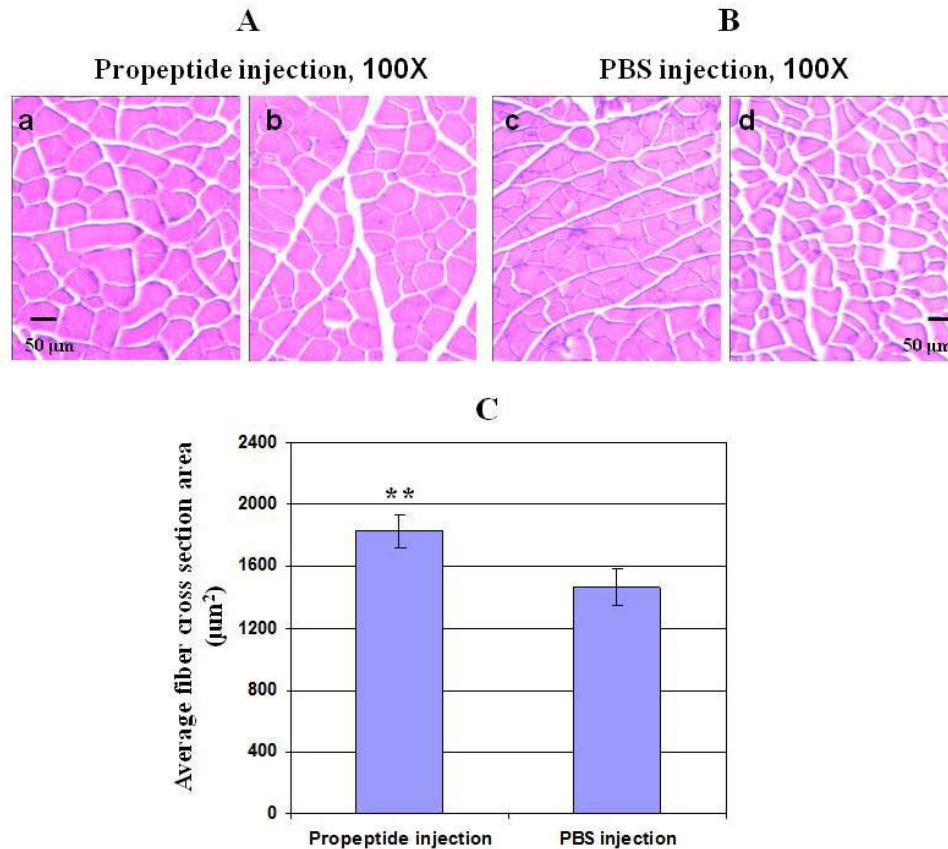


Figure 2.6 Muscle histology analyses of mice injected with mutated pig myostatin propeptide or PBS. The muscle cross-sections of two mice (a and b) that were randomly selected from the propeptide injection group are shown in **A** while the muscle cross-sections two mice (c and d) that were randomly selected from the PBS injection group are shown in **B**. Average muscle fiber cross section area between propeptide injection group (n=4) and PBS injection group (n=4) was compared in **C**. Data are present as mean \pm SEM, means between propeptide injection group and PBS injection group differ at $P < 0.01$ (**).

CHAPTER 3

SUPPRESSION OF GROWTH DIFFERENTIATION FACTOR 11

BY TRANSGENIC OVER-EXPRESSION OF ITS PROPEPTIDE IN SKELETON

3.1. Abstract

Growth differentiation factor 11 (GDF11), which is also called bone morphogenetic protein 11 (BMP11), plays an essential role in skeletal formation. One of the potential GDF11 antagonists, GDF11 propeptide, has been demonstrated to inhibit GDF11 activity *in vitro*. However, the *in vivo* effect of GDF11 propeptide on blocking GDF11 function has not yet been reported. To study the function of GDF11 propeptide in bone growth by down-regulating GDF11 function, we produced transgenic mice over-expressing GDF11 propeptide under the control of an osteoblast-specific promoter. The transgenic mice showed formation of extra ribs on the seventh cervical vertebra (C7), suggesting a homeotic transformation of the C7 vertebra into a thoracic vertebra. The mRNA of GDF11 propeptide transgene was detected as early as at 12.5 dpc in embryonic skeleton, and a higher transgene expression level was associated with a higher frequency of C7 rib formation. Over 80% of the transgenic mice from a line expressing the transgene at a high level displayed additional ribs on C7. The transgene also caused anterior shifts of the anterior expression boundary of Hoxa-4 and Hox-5 genes from their normal prevertebra locations in 13 dpc transgenic embryos. Furthermore, bone mineral content, bone mineral density and relative trabecular bone volume was significantly increased by 11.12%, 9.68% and 60.9%, respectively, in adult transgenic male mice, and 14.96%, 8.69% and 57.7%, respectively, in adult female transgenic mice, compared to their sex-matched wild-type

littermates. These results suggest GDF 11 play an important role in embryonic vertebral formation as well as postnatal bone development.

3.2. Introduction

Growth differentiation factor 11 (GDF11) plays essential roles in bone growth. Factors that modulate the signaling of GDF11 may also function to regulate bone growth.

The regulation of GDF11 signaling appears similar to that of its close TGF- β member, GDF-8 (myostatin). The gene of GDF11, like myostatin, encodes for three domains, including an N-terminal signal peptide, a propeptide and a C-terminal peptide, which is the mature GDF11 ligand (Gamer et al., 1999; Nakashima et al., 1999; Ge et al., 2005). Similar with myostatin processing, after the removal of signal peptide, GDF-11 precursor protein is believed to be severed by a furin-like proprotein convertase, PC5/6, at the conserved RSRR site to separate the GDF11 propeptide from mature GDF11 protein (Ge et al., 2005 and Essalmani et al., 2008). The GDF11 propeptide can bind to mature GDF11 protein to form a latent complex that can be activated by BMP1/Tolloid (TLD)-like metalloproteinases via cleavage of the propeptide in the latent complex (Ge et al., 2005). In addition to its propeptide, GDF-11 also is inhibited by a BMP antagonist, follistatin (Gamer et al., 1999). GDF11 was believed to signal through type 1 receptor ALK5, activin type II receptors -A and -B (Oh and Li, 1997; Oh et al., 2002 and Andersson et al., 2006). Based on the pathway of GDF11 signaling, it seems that GDF11 propeptide, follistatin, and mutant GDF11 receptors are possible GDF11 antagonist. However, follistatin or mutant GDF11 receptors may also have the ability to interfere with the signaling of other BMP members, since follistatin has been shown to be capable of binding to BMP-2, -4 and -7 (Iemura et al., 1998) and all the known GDF-11 receptors are also shared by many other

BMPs (Caestecker, 2004). This suggests that only GDF-11 propeptide may specifically down-regulate GDF11 function.

GDF-11 propeptide has been demonstrated to effectively antagonize GDF-11 signaling in cultured A204 cells (Ge et al., 2005). However, the tested GDF11 propeptide was a recombinant propeptide carrying a fusion protein in the C-terminal end and a modified signal peptide in the N-terminal end, raising the question whether the native GDF11 propeptide also can inhibit GDF11 activity. More importantly, although recombinant GDF11 propeptide was shown to block GDF11 activity in vitro, it is still unknown whether GDF11 propeptide can depress GDF11 function in vivo. To answer these two questions, we decided to investigate the in vivo effects of normal GDF11 propeptide on suppressing GDF11 function. Considering that the primary function of GDF11 is to regulate bone formation, we generated transgenic mice over-expressing GDF11 propeptide under the control of a bone-specific promoter, 2.3 kb alpha 1 type 1 collagen promoter (Rossert et al., 1995; Dacquin et al., 2002), and analyzed the skeletal phenotype of the transgenic mice.

3.3. Materials and Methods

3.3.1. Construction of transgene Plasmid and production of transgenic mice

The cDNA of mouse GDF11 propeptide (encoding for 1-296 AA) was amplified from a synthetic clone (Openbiosystems, CA, Catalog No.: OMM4760-99847460; Gene bank accession No.: BC152721) by PCR. A stop codon (TAA) was added to the end of the gene and two BamH I sites were added to the flanking regions of the gene during PCR. Amplified GDF 11 propeptide gene was cloned into the TA vector pCR4-TOPO (Invitrogen, CA) and then the gene was cut out by BamH I to replace the lacZ gene between the mouse 2.3-kb α 1 type 1 collagen promoter (Rossert et al., 1995; Dacquin et al., 2002) and mouse protamine 1 poly A signal in the pJ251

plasmid (a kind gift from Dr. Crombughe, University of Texas). The transgene expression cassette (promoter + GDF11 propeptide cDNA + poly A signal sequence) was digested with Kpn I and EcoR V and inserted into the multiple cloning sites of pENTR1A (Invitrogen) to generate plasmid pENTR1A-mGDF11-pro. After a LR recombination reaction (Gateway Technology, Invitrogen) between plasmids pENTR1AmGDF11-pro and pmGENIE-2 which is a helper-independent plasmid for piggyBac transposon-mediated gene transfer (Urschitz et al., 2010), the transgene expression cassette was cloned into the piggyBac transposon in pmGENIE-2 to generate plasmid pmGENIE-2-mGDF11-pro. Using the plasmid pmGENIE-2-mGDF11-pro, transgenic mice were produced by intracytoplasmic sperm injection (ICSI) technique as described (Urschitz et al., 2010).

3.3.2. Identification of transgenic mice

Transgenic mice were identified by PCR amplification of a 381 bp fragment on the genomic DNA isolated from mouse tail tissue, with P1 and P2 primers. Their positions in transgene expression cassette were indicated in Figure 3.1A, their sequences are as follows. P1: 5'-GTCACATCCGTATCCGTTCACCT-3'; P2: 5'-AGCCCTCTACTTACTTCGCCTC-3'. The amplified 381bp DNA fragment covers the junction of GDF-11 propeptide cDNA and Protamine 1 PolyA signal sequence. To rule out possible false negative PCR results, we also used the same tail genomic DNA samples to run PCR amplifications of a 340 bp fragment of mouse β -actin gene with a set of primers (their sequences are as follows. Forward: 5'-TTGAGACCTTCAACACCCC-3'; Reverse: 5'-TTGCCAATAGTGATGACCTG-3'). Four PCR products that were amplified from the tail genomic DNA of PCR-positive transgenic mice were randomly selected for DNA sequencing. The sequencing results were used to validate the

identity of PCR-amplified transgene in accordance with the sequence in transgene plasmid pmGENIE-2-mGDF11-pro.

3.3.3. Analyses of transgene expression

Real-time PCR was performed as previously described (Li et al., 2009). Briefly, total RNA was extracted from tested tissues of 5-week-old mice and then treated with DNase to eliminate any contaminating genomic DNA followed by synthesis of the first strand cDNA. Expression level of the transgene was analyzed by real-time PCR amplification of a 105 bp fragment on synthesized first strand cDNA, with P3 and P4 primers (their positions in transgene expression cassette see Figure 3.1A, and their sequences are as follows. P3: 5'-

TTTCATGGAGCTCGAGTCCTAGA-3'; P4: 5'-ATCTGCTCCTGCTTTTGCTGC-3').

Expression level of a housekeeping gene, glyceraldehyde-3-phosphate dehydrogenase (GAPDH) was also measured with a set of primers (their sequences are as follows. Forward: 5'-

GCAGTGGCAAAGTGGAGATTG-3'; Reverse: 5'-CCGTGAGTGGAGTCATACTGGAA-3')

during real-time PCR and used as an endogenous control. Calculation of relative expression of transgene followed the $2^{-\Delta\Delta C_t}$ method. To detect the starting time of transgene expression in embryo, reverse transcription PCR was used. Embryos were collected at 10.5 dpc, 12.5 dpc, 14.5 dpc and 16.5 dpc. Muscle tissues were dissected from embryos and used for DNA isolation and genotyping. Total RNA was extracted from the whole tail tissue of transgenic embryos and treated with DNase to eliminate any genomic DNA contamination followed by the synthesis of the first strand cDNA. Expression of the transgene at different embryonic stage was detected by reverse transcription PCR with a same amount of cDNA as template and the same set of primers (P1 and P2) that are used for PCR genotyping. GAPDH gene was used as internal control and it was amplified by a set of primers (forward: 5'-GTGCTGAGTATGTCGTGGAG-3', located on

exon 3; reverse: 5'-GTCTTCTGGGTGGCAGTGAT-3', located on exon 5). The amplification product of GAPDH from the cDNA is 295 bp.

3.3.4. Alizarin red and alcian blue staining of skeleton

Mice were euthanized, skinned, eviscerated and dehydrated in 95% ethanol for 4 days followed by incubation in acetone for 3 days to remove fat. Specimens then were stained for 3 days in alizarin red and alcian blue staining solution containing 70% ethanol, 8% glacial acetic acid, 0.001% alcian blue and 0.0005% alizarin red. After staining, specimens were cleared in 1% KOH until skeletons were clearly visible through the surrounding tissues. Specimens then were placed in solution containing 1% KOH and 20% glycerol until the surrounding tissues were completely leached, and then were transferred to 50% glycerol followed by 80% glycerol over several days and stored in 100% glycerol.

3.3.5. *In situ* hybridization

Embryos at 13 dpc were collected from pregnant wild-type female mice that were mated with transgenic male mice (from line 353). A piece of tail tissue was taken from each embryo to isolate DNA for PCR genotyping. Five wild-type embryos and five transgenic littermate embryos were fixed in 4% paraformaldehyde, embedded in OCT and sagittal cryostat sections (10 μ m) were taken. Digoxigenin-labeled Hoxa-4 and Hoxa-5 riboprobes were synthesized using the DIG RNA labeling kit (Roche, Germany. Cat No: 11 175 025 910). The template plasmids for probe synthesis (Kawazoe et al., 2002) were kindly provided by Dr. Mastake Araki (Kumamoto University, Japan). *In situ* hybridization was carried out using the digoxigenin labeled riboprobes on frozen sections as described (Takahara et al., 1997). After stopping the color reaction, sections were counterstained with fast green and mounted with paramount and observed under microscopy.

3.3.6. Analysis of ossification in embryos

Two litters of 16.5 dpc embryos were collected from pregnant wild-type female mice that were mated with transgenic male mice (from line 353). Skeletons of the embryos from the same litter were stained with the same alizarin red and alcian blue staining solution.

3.3.7. X-ray analyses of body composition and bone mineral

Ten week-old mice from transgenic lines 353 and 337 were killed, weighted, stored in dry ice and sent for scanning by dual energy X-ray absorptiometry (DXA). The DXA instrument used in this study was the PIXImus small animal DXA system (Lunar Corporation). The muscle mass, total bone mineral content, bone area and bone mineral density were measured as described by Mitchell and Wall (2007).

3.3.8. Measurement of the length of forelimb bones

The left forelimb was dissected from terminated 10 week-old mice from transgenic lines 353 and 337 and stained with alizarin red and alcian blue, the length of the ulna bone and the humerus bone then were measured with a slide caliper.

3.3.9. Histology analysis of bone volume

The femora were dissected from euthanized 3 month-old mice, fixed in 4% paraformaldehyde at 4°C for 24h, washed with PBS, stored in 70% ethanol, embedded in glycol methacrylate and 7-10 µm sections were cut by microtome. The sections were stained by Von Kossa method that can detect the deposits of calcium or calcium salt. Stained sections were observed under the microscopy and images of the sections were captured with a camera connected to the microscope. Section images were then analyzed by the BioQuant image analysis system. Relative trabecular bone volume (trabecular bone volume / tissue volume, %) was measured in the bone marrow cavity area between 0.5 mm to 2mm away from the growth plates.

3.3.10. Statistical analysis

Data were analyzed by SAS 9.2 program (SAS Institute, Cary, NC), and the two samples t-test for means program was used for mean comparisons in Table 3.2, Table 3.3 and Figure 3.7. Data are present as mean \pm standard error of mean (SEM) or mean \pm standard deviation (SD). Significant difference of means between two different groups was determined at $P < 0.05$ (*) or $P < 0.01$ (**).

3.4. Results

3.4.1. Production of transgenic mice

The transgene expression cassette was constructed as shown (Figure 3.1A). Transgenic mice were generated by intracytoplasmic sperm injection (ICSI) technique in combination with piggyBac transposon-mediated gene transfer. A total of 657 mouse oocytes from strain B6D2F1 were injected with sperm heads that were mixed with the transgene plasmid. A total of 382 injected oocytes developed into 2-cell embryos, which were transferred into surrogate mothers. Forty-four mice were delivered, among them 19 transgenic founder mice were identified by PCR (Figure 3.1B). The transgenic mice were viable and fertile. Fourteen lines of transgenic mice were established after breeding the 19 adult transgenic founder mice with wild-type mice.

3.4.2. Expression of transgene in transgenic mice

The mRNA levels of GDF11 propeptide transgene were detected in tail tissue because the alpha1 type 1 collagen promoter used for controlling the transgene expression is highly active in tail tissue (Rossert et al., 1995). The mRNA levels of GDF11 propeptide transgene were detected in all the 19 transgenic founders at the age of 5 weeks. The expression levels of the transgene varied significantly among different transgenic founders (Figure 3.2A). In two founder mice (352

and 353), the transgene mRNA abundance was approximately 800-1200 times of that in founder 334, which had the lowest level of transgene expression (Figure 3.2A). The relative transgene expression level in the offspring was very similar with that detected in their transgenic founder mice. For example, the relative transgene expression level in founder 353, 337 and 339 was 953.05 ± 209.15 : 261.27 ± 37.06 : 62.01 ± 7.11 (see figure 3.2A), which was equal to 15.37 ± 3.37 : 4.21 ± 0.60 : 1.00 ± 0.11 . In the offspring from these 3 transgenic lines, the relative transgene mRNA level that was measured in tail tissue at 5 weeks of age, was 18.56 ± 4.75 : 6.24 ± 1.19 : 1.0 ± 0.8 (n=3 in each lines).

To investigate the tissue specificity of transgene expressions, we analyzed the transgene expressions in bone and several other tissues. A high transgene mRNA level was detected in calvaria bone compared with muscle, fat, brain, lung, heart, liver and kidney (Figure 3.2B). The GDF11 propeptide transgene also was highly expressed in tail and tooth tissues of transgenic mice (Figure 3.2B). This is consistent with the data from the study that reported the 2.3kb alpha 1 type 1 collagen promoter is also highly active in caudal vertebrae and tooth, which contains osteoblasts and osteoblast-like odontoblasts, respectively (Rossert et al., 1995). The transgene mRNA was detectable in tail tissue by reverse transcription PCR at 12.5 dpc and later times (14.5 and 16.5 dpc), but there was no transgene expression in 10.5 dpc transgenic embryos (Figure 3.2C).

3.4.3. Skeletal abnormalities in transgenic mice

To reveal the effects of transgene on animal bone development, we stained the skeletons of both transgenic mice and their wild-type littermates with alizarin red and alcian blue. Transgenic mice have abnormal skeletons that present homeotic transformation of vertebra. As shown in

Figure 3.3A, the transgenic mice had 14 pairs of ribs, which is one more pair of ribs than their wild-type littermates. The extra ribs in the transgenic mice were caused by forming ectopic ribs on the seventh cervical vertebra (C7) instead of inserting an additional thoracic vertebra into the vertebral column (Figure 3.3B). The additional rib, also called the cervical rib, did not attach to the sternum independently like the normal vertebrosteral ribs, but fused to the middle of the rib that is articulated with the first thoracic vertebra (T1) in the transgenic mice (Figure 3.3B). In some cases, the C7 rib was shown on only one side (TG-unilateral) while in other cases exhibited on both sides (TG-bilateral) of the anterior/posterior axial skeleton of the transgenic mice (Figure 3.3C). Analysis on the lumbar, sacral and caudal regions of the anterior/posterior axial skeleton indicated that the vertebrae in these regions were normal in the transgenic mice (data not shown).

The effect of the GDF11 propeptide transgene on the patterning of the anterior/posterior axial skeleton was dose or expression level-dependent. The frequency (81.8%) of the formation of C7 ribs in transgenic mice from the high-expression line 353 was much higher than that in transgenic mice from lines 337 and 339 expressing a lower level of transgene (Table 3.1).

To investigate whether the transgene affects the appearance of the C7 vertebral body, we analyzed the vertebral bodies of the C7 and two neighbor vertebrae, the C6 and T1. In wild-type mice, although the C7 vertebral body does not have tuberculi anterior and the transverse foramen which are markers of the C6 vertebral body, the morphology of the C7 vertebral body resembles that of the C6 vertebral body rather than that of the T1 vertebral body (Figure 3.4). However, in transgenic mice, especially in those displaying cervical ribs on both sides of the C7 (TG-bilateral), the C7 vertebral body tended to transform into a vertebral body resembling the T1 vertebral body (Figure 3.4).

In the GDF11 propeptide transgenic mice, extra ribs were formed on C7, which implied a homeotic transformation of the C7 into a thoracic vertebra. However, the manner of the attachment between the C7 ribs and the C7 vertebral body was different from that between the T1 ribs and the T1 vertebral body. The C7 ribs were articulated with the C7 vertebral body through only one contact point while the T1 ribs were articulated with the T1 vertebral body by two contact points (Figure 3.4). This result seems to suggest that the C7 vertebra in the transgenic mice was not wholly but partially transformed into a T1 vertebra.

3.4.4. Expressions of *Hoxa-4* and *Hoxa-5* genes in transgenic mice

The axial vertebral patterning is thought to be controlled by the spatially restricted expression patterns of *Hox* genes (Favier and Dolle, 1997; Mark et al., 1997; Wellik, 2007). Targeted disruptions of *Hoxa-4* and *Hoxa-5* genes in mice result in ectopic formation of ribs on C7 (Jeannotte et al., 1993; Horan et al., 1994), which was very similar to that in the GDF11 propeptide transgenic mice. Homozygous *rac28*-deficient mice exhibiting the same posterior transformation of the C7 into T1 as seen in the GDF11 propeptide transgenic mice also showed altered expression patterns of *Hoxa-4* and *Hoxa-5* genes (Takahara et al., 1997). These results imply that misexpression of *Hoxa-4* and *Hoxa-5* genes may be involved in ectopic formation of C7 ribs. To determine whether changes in expression patterns of *Hox* genes were responsible for the vertebral transformation in the transgenic mice, we examined the expression patterns of *Hoxa-4* and *Hoxa-5* genes. *In situ* hybridization analysis showed that the anterior boundaries of *Hoxa-4* and *Hoxa-5* gene expression were shifted anteriorly by 1 prevertebra in 13-dpc-embryos of the transgenic mice compared to their wild-type littermates (Figure 3.5). The anterior boundary of *Hoxa-4* gene expression was detected on the second prevertebra (PV2) in wild-type mice, however, it was detected on the first prevertebra (PV1) in transgenic embryos (Figure 3.5).

There was also a shift of anterior boundary of Hoxa-5 gene expression from the fourth prevertebra (PV4) in the wild-type embryos to the third prevertebra (PV3) in transgenic embryos (Figure 3.5).

3.4.5. Ossification in transgenic mice

To examine the effects of transgene on bone mineralization, two litters of 16.5 dpc-old embryos were analyzed by alizarin red and alcian blue staining. As shown in Figure 3.6, ossification of bone occurred earlier in 16.5 dpc-old transgenic mice than that in their wild-type littermates.

3.4.6. Body mass, muscle mass, total bone mineral content, bone area and bone mineral density in transgenic mice

To determine whether the transgene affects the growth of transgenic mice, body mass, muscle mass, and several bone parameters, including total bone mineral content, bone area and bone mineral density were measured in 10 week-old wild-type mice and their transgenic littermates. As shown in Table 3.2, male and female transgenic mice were 1.77g (or 7.87%) and 1.96g (or 11.04%), respectively, heavier than their sex-matched wild-type littermates. The muscle mass in the male and female transgenic mice also was increased by 1.91g (or 11.86%) and 1.47g (or 11.50%), respectively (Table 3.2). It seems the heavier body mass in the transgenic mice was mainly caused by increase in muscle mass, as the increased muscle mass almost could account for the entire increase of body mass. Total bone mineral content in male and female transgenic mice increased by 11.12% and 14.96%, respectively, compared to their sex-matched wild-type littermates (Table 3.2). Bone area was not different between transgenic and wild-type male mice or female mice (Table 3.2). Bone mineral density in transgenic male and female mice was increased by 9.68% and 8.69%, respectively (Table 3.2).

3.4.7. Increase of bone volume in transgenic mice

To further examine the changes of bone growth in transgenic mice, relative trabecular bone volume was analyzed by histology on femorus bone of 3 month-old wild-type and transgenic mice. Transgenic mice had more trabecular bone than their wild-type littermates (Figure 3.7A). The relative trabecular bone volume was significantly increased from 11.5% in wild-type male mice to 18.5% in transgenic male mice, and from 10.4% in wild-type female mice to 16.4% in transgenic female mice (Figure 3.7B). In other words, the trabecular bone volume was increased by 60.9% and 57.7%, respectively, in male and female transgenic mice.

3.4.8. The length of bones in forelimb of transgenic mice

To investigate whether there are changes in length of limb skeleton in transgenic mice, the length of two forelimb bones were measured in 10 week-old transgenic and wild-type mice. As shown in Table 3.3, there was no difference in the lengths of the ulna bone and the humerus bone, between 10 week-old wild-type mice and their transgenic littermates.

3.5. Discussion and Conclusions

Although GDF11 propeptide was shown to inhibit GDF11 activity in vitro, its in vivo effect on blocking GDF11 function has not yet been reported. The results from this report demonstrated that transgenic over-expression of GDF11 propeptide under the control of a skeleton-specific promoter, resulted in abnormal anterior/posterior axial skeleton. The transgenic mice displayed ectopic formation of ribs on C7. The skeleton defect in the transgenic mice was similar with, but less severe than that in homozygous GDF11-deficient (GDF11^{-/-}) mice. The transgenic mice, unlike the GDF11^{-/-} mice, showed normal vertebrae in the lumbar, sacral and caudal regions. One possible reason for this is GDF11 function was incompletely depressed by the product of the GDF 11 propeptide transgene. Skeletally over-expressed GDF11 propeptide

probably resulted in a partial suppression of GDF11 activity in the skeleton, which might still allow the transgenic mice to develop normal lumbar, sacral and caudal vertebrae.

In GDF11^{-/-} mice, vertebra transformation also occurred on C7. However, the C7 was transformed into a vertebra whose morphology resembles a more anterior vertebra, the C6 vertebra (McPherron et al., 1999). This is different from that in transgenic mice generated in this report, in which the C7 tend to convert into a more posterior vertebra, the T1 vertebra (Figure 3.4). Recently, myostatin was found redundant to GDF11 in regulating the patterning of axial vertebrae (McPherron et al., 2009). Furthermore, myostatin function could be suppressed by GDF11 propeptide (Ge et al., 2005). Therefore, we suspected that the functions of both GDF-11 and myostatin were depressed in the skeletons of transgenic mice by over-expressed GDF11 propeptide. This might be the reason that caused the C7 vertebra in the transgenic mice to transform into a T1-like vertebra rather than a C6-like vertebra, which was the case in GDF11^{-/-} mice.

The results of changes in expression of two Hox genes in the transgenic mice offered some insights about the downstream regulatory events of GDF11 propeptide. Precise regulation of the expression boundaries of Hox genes is critical for specifying the segment identities along the anterior/posterior axis (Manak and Scott, 1994). In the GDF11-knockout mice, it was shown that GDF11 acts as an upstream molecule to regulate the expression pattern of Hox genes, whereby controlling the pattern of the anterior/posterior axial skeleton (McPherron et al., 1999). Consistent with this mechanism, anterior displacements of the anterior expression boundaries of Hoxa-4 and Hoxa-5 genes along the anterior/posterior axis were detected in 13 dpc transgenic embryos in this report (Figure 3.5). This result not only suggest that GDF11 propeptide signals through Hox genes to regulate vertebral formation via down-regulating GDF11 function, but

also imply that altered expression patterns of Hoxa-4 and Hoxa-5 genes are involved in ectopic formation of ribs on C7.

Mammals have remarkably constant seven cervical vertebrae. The lack of variation in cervical vertebrae number among different mammalian animals is primarily due to developmental constraints. Any changes in the number of cervical vertebrae are coupled with neural problems and an increased susceptibility to early childhood cancer and stillbirths (Galis, 1999). The formation of ribs on C7, which indicates a partially or wholly homeotic transformation of the C7 into a thoracic vertebra, reduces the number of cervical vertebrae. In human, the alteration in cervical vertebrae number, which results from the formation of C7 cervical ribs, was reported to associate not only with thoracic outlet syndrome, the compression of the branchial nerves and blood vessels entering the limbs by cervical ribs (Makhoul and Machleder, 1992; Roos, 1996), but also with increased risk of early childhood cancer (Schumacher et al., 1992; Galis, 1999). The formation of the cervical ribs on C7 in the transgenic mice produced from this study may imply that malfunction of GDF11 propeptide might be related to occurrences of thoracic outlet syndrome or childhood cancer.

Studies have shown that many BMP members and their inhibitors are important in regulation of bone mineral content, bone mineral density and bone volume during postnatal bone growth (Daluisi et al., 2001; Devlin et al., 2003; Gazzero et al., 2005; Kugimiya et al., 2005). GDF11, as a member of the BMP family, may also participate in regulating postnatal bone growth. The results from this study showed that inhibition of GDF11 function by skeleton-specific over-expression of its propeptide significantly increased the bone mineral content, bone mineral density and relative trabecular bone volume in the transgenic mice (Table 3.2 and Figure 3.7), implying GDF11 propeptide may play important roles in postnatal bone formation by

inhibiting GDF11 function. Furthermore, our data showed that, even during the late embryonic stage, GDF11 propeptide seems to start to initiate mineral deposition in bone, and we observed that ossification occurred earlier in 16.5 dpc transgenic mice than that in their wild-type littermates (Figure 3.6). This suggests that suppression of GDF11 function in osteoblasts by its propeptide may facilitate or enhance bone mineralization.

The GDF11 propeptide transgene seems not only regulated bone formation and development but also acted on muscle growth, since muscle mass in the transgenic mice was significantly increased by 11.5-11.86% (Table 3.2). GDF 11 propeptide has been indicated to suppress the function of a significant negative regulator for muscle growth, myostatin (Ge et al., 2005). Therefore, we believe that increased muscle mass in the transgenic mice might result from the depression of myostatin function by the over-expressed transgene. Our data already showed that the transgene had a low expression in muscle tissue (Figure 3.2 B). This weak expression of GDF11 propeptide transgene in muscle tissue might down-regulated myostatin activity and thereby caused increase of muscle growth in transgenic mice. However, the increased muscle mass in transgenic mice also could be caused by another possibility in that some amount of skeletally over-produced GDF11 propeptide was transported to muscle tissue to inhibit myostatin function.

It has been demonstrated that administration of GDF11 to early wing bud caused dramatic shortening of limb skeleton in chicken embryos (Gamer et al., 2001), suggesting GDF11 probably normally functions to limit the length of limb skeleton. Therefore, down-regulation of GDF11 function might result in increase of limb skeleton length. However, we observed no change in the length of limb skeleton of the GDF11 propeptide transgenic mice in comparison with their wild-type littermates (Table 3.3). The activity of chondrogenesis in the cartilage of

epiphyseal growth plate is responsible for determining the length of the long bone. The dramatic truncation of limb skeleton in GDF11-treated chicken embryos was believed to be mainly due to the strong negative effects of GDF11 on chondrogenesis (Gamer et al., 2001). In the transgenic mice generated from the present study, expression of the GDF11 propeptide transgene was driven by an osteoblast-specific promoter, which is inactive in cartilage. Therefore, the transgene in the transgenic mice might have little effects on chondrogenesis activity in the growth plate of long bone and thus have no effects on increasing the length of limb skeleton.

In conclusion, skeletal over-expression of GDF11 propeptide resulted in homeotic transformation of the seventh cervical vertebra into a thoracic vertebra. The effect of the transgene on vertebral formation was expression level-dependent. Expression of the GDF11 propeptide transgene appeared to start at the late embryonic stage. The transgene caused expression shifts of Hoxa-4 and -5 genes from their normal prevertebra locations in 13 dpc embryos. Bone mineral content, bone mineral density and relative trabecular bone volume were significantly increased in adult transgenic mice. These results suggest that GDF11 propeptide not only regulate vertebral formation through the GDF11/Hox genes pathway, but also plays important roles in postnatal bone growth. The GDF11 propeptide transgenic mouse is a useful animal model for understanding the regulation of GDF11 propeptide in bone development and growth.

Table 3.1 Skeletal analysis of wild-type and transgenic littermates from different lines#

	Line 353		Line 337		Line 339	
	WT	TG	WT	TG	WT	TG
No. of analyzed mice	24	23	23	21	21	20
No. of mice with unilateral C7 rib	0	14	0	4	0	2
No. of mice with bilateral C7 ribs	0	4	0	0	0	1
Frequency of forming C7 ribs	0	81.8%	0	19.0%	0	15.0%

#Skeletons of 4 -5 litters of 1-day-old mice from each line were analyzed by alizarin red and alcian blue staining after PCR genotyping. The relative transgene expression ratio in transgenic offspring mice from lines 353, 337 and 339 is $18.56 \pm 4.75 : 6.24 \pm 1.19 : 1.0 \pm 0.8$ (n=3 in each lines), which is similar with the relative transgene expression ratio in founders 353, 337 and 339, which is $953.05 \pm 209.15 : 261.27 \pm 37.06 : 62.01 \pm 7.11$ (see figure 3.2A), which is equal to $15.37 \pm 3.37 : 4.21 \pm 0.60 : 1.00 \pm 0.11$.

Table 3.2 Body mass, muscle mass, total bone mineral content, bone area and bone mineral density of 10 week-old wild-type mice and their transgenic littermates#

	Male			Female		
	Wild-type (n=12)	Transgenic (n=9)	Increase (%)	Wild-type (n=16)	Transgenic (n=14)	Increase (%)
BM (g)	22.56±0.61	24.33±0.27*	7.87	17.80±0.44	19.76±0.39**	11.04
MM (g)	16.09±0.45	18.00±0.25**	11.86	12.83±0.34	14.30±0.30**	11.50
BMC (g)	0.350±0.016	0.389±0.006*	11.12	0.297±0.017	0.341±0.011*	14.96
BA (cm ²)	7.262±0.199	7.412±0.181	2.07	6.712±0.259	7.119±0.114	6.06
BMD (mg/cm ²)	48.00±1.28	52.64±1.22*	9.68	43.79±1.23	47.59±0.93*	8.69

BM=Body mass, MM=Muscle mass, BMC=Bone mineral content, BA=Bone area, BMD=Bone mineral density. Values are presented as mean ± SEM. The means between wild-type male group and transgenic male group, and the means between wild-type female group and transgenic female group differ at P<0.05 (*) and P<0.01(**).

Table 3.3 Length of the ulna bone and the humerus bone in forelimb of 10 week-old wild-type mice and their transgenic littermates#

	Male		Female	
	Wild-type (n=13)	Transgenic (n=14)	Wild-type (n=7)	Transgenic (n=7)
Length of the ulna bone (mm)	13.49 ± 0.13	13.51 ± 0.12	13.16 ± 0.14	12.96 ± 0.30
Length of the humerus bone (mm)	11.53 ± 0.10	11.49 ± 0.15	10.97 ± 0.21	11.06 ± 0.25

#Values are presented as mean ± SEM. The means between wild-type male group and transgenic male group, and the means between wild-type female group and transgenic female group were not different (P>0.05).

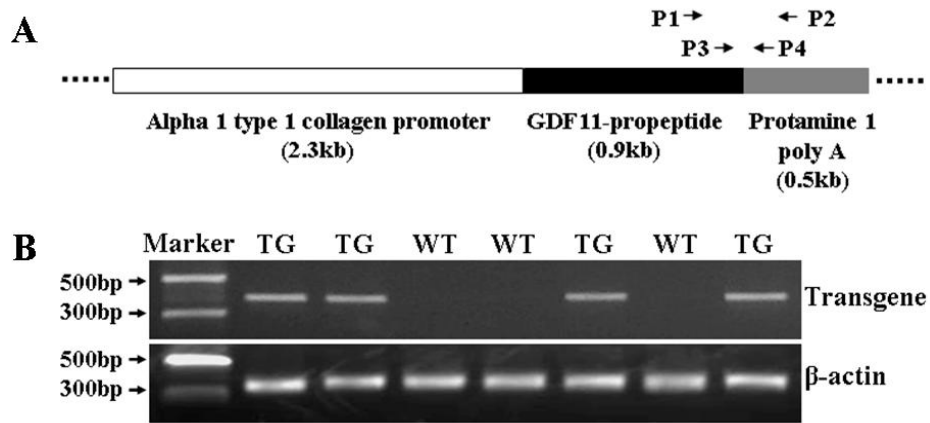


Figure 3.1 Production of transgenic mice. **A:** The schematic construct of transgene expression cassette and design of primers for analyzing the transgenic mice. P1 and P2 are used for PCR genotyping and reverse transcription PCR while P3 and P4 are used for quantitative real-time PCR; **B:** The representative results from PCR genotyping. TG = transgenic, WT= wild type.

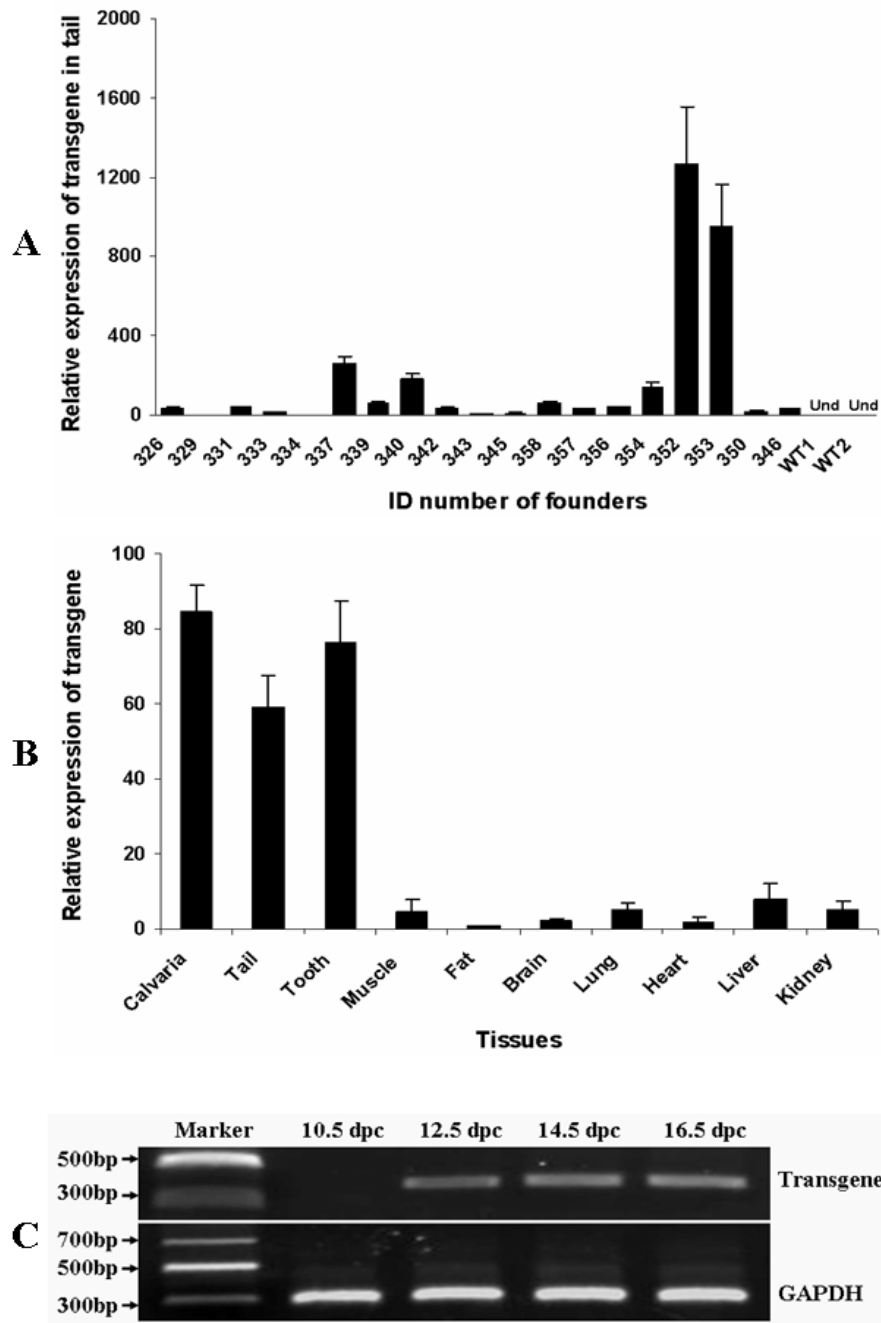


Figure 3.2 Expression of transgene in transgenic mice. **A**: Analysis of transgene expression levels in tail tissues of transgenic founders by relative quantitative real-time PCR at 5 weeks of age. WT = wild-type. Und = undetectable. Real-time PCR was performed three times. Data are presented as mean \pm SD. Expression levels of transgene in all the transgenic founders were

normalized to the founder with the lowest expression of transgene (founder 334, its expression level of transgene was defined as 1); **B**: Analysis of transgene expression levels in different tissues of transgenic mice by relative quantitative real-time PCR at the age of 5 weeks. Real-time PCR was performed on 3 transgenic littermates of line 353. Data are presented as mean \pm SD. Expression levels of transgene in all tested tissues were normalized to the tissue with the lowest expression of transgene (fat tissue, its expression level of transgene was defined as 1); **C**: Detections of transgene expression in tail tissues of transgenic mice at different embryonic stages by reverse transcription PCR. dpc = days post coitum.

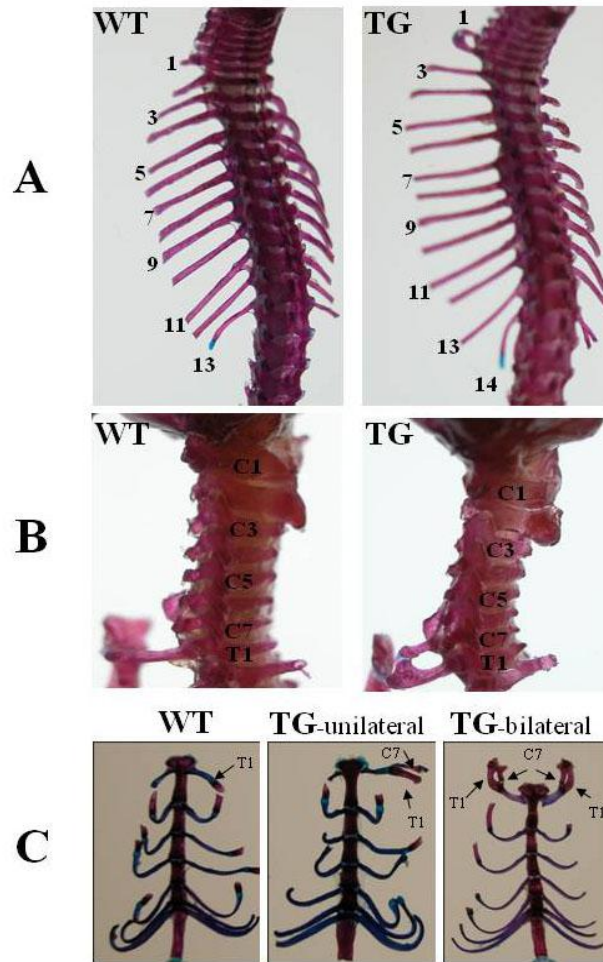


Figure 3.3 Abnormalities in the anterior/posterior axial skeleton of transgenic mice. Skeletons of 10-day-old mice were stained with alizarin red and alcian blue. **A:** Dorsal view of thoracic vertebrae in wild-type (WT) and transgenic (TG) mice, showing TG mice have 14 pairs of ribs while WT mice have 13 pairs of ribs; **B:** Lateral view of cervical vertebrae in WT and TG mice, showing an extra rib in TG mice is formed on the seventh cervical vertebra (C7). This C7 rib is fused to the middle of the rib that is articulated with the first thoracic vertebra (T1) and attached to the sternum together at the T1 position in TG mice; **C:** Ventral view of vertebrosteral ribs in WT and TG mice, showing the C7 rib which is fused to the T1 rib, in some cases, is on only one side (TG-unilateral) but in some other cases is on both sides (TG-bilateral) of the TG mice.

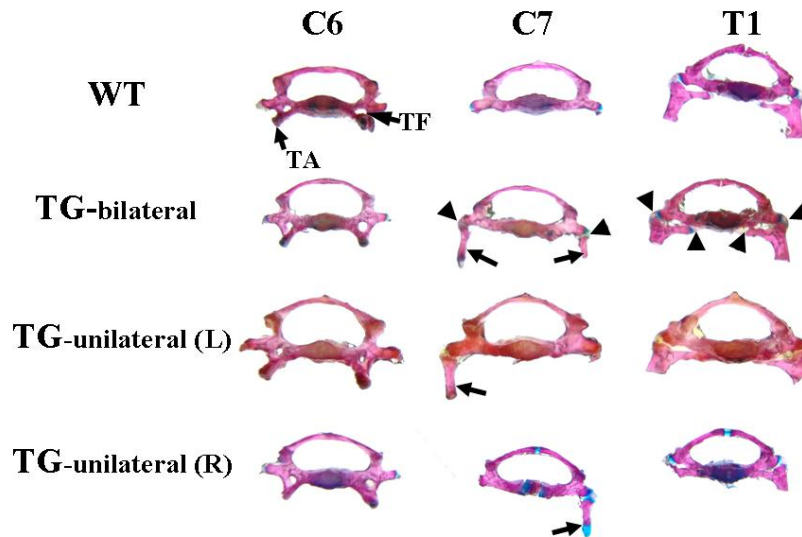


Figure 3.4 Changes in morphological appearance of the seventh cervical vertebra in transgenic mice. Vertebrae were dissected from alizarin red and alcian blue-stained skeleton of 1-3 week-old mice. Note that, in wild-type (WT) mice, the C7 vertebral body resembles the C6 vertebral body instead of the T1 vertebral body, but without the tuberculi anterior (TA) and the transverse foramen (TF) that characterize the C6. In transgenic mice (TG) with ribs on C7, the C7 vertebral body resembles the T1 vertebral body instead of the C6 vertebral body. This is more obvious in TG-bilateral mice. Also note that, in TG-bilateral, TG-unilateral (L) and TG-unilateral (R) mice, there is only one contact point between the C7 ribs (indicated by arrows) and the C7 vertebral body while there are two contact points between the T1 ribs and the T1 vertebral body. The contact points between ribs and vertebral bodies are indicated with arrowheads only in TG-bilateral but not in TG-unilateral (L) and TG-unilateral (R) mice. TG-bilateral = transgenic mice showing C7 ribs on both sides; TG-unilateral (L) = transgenic mice showing C7 rib on the left side; TG-unilateral (R) = transgenic mice showing C7 rib on the right side.

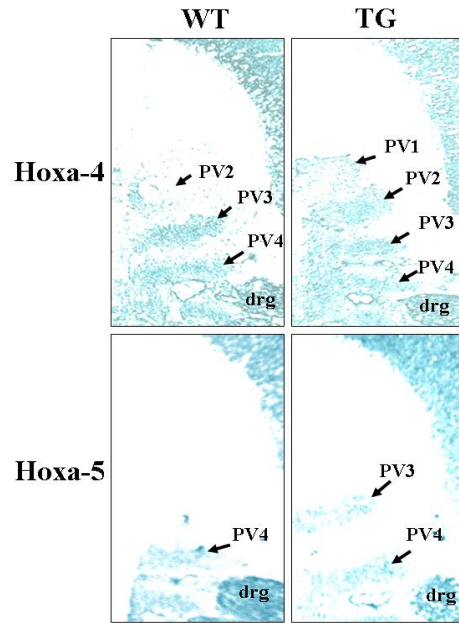


Figure 3.5 Altered expression patterns of Hoxa-4 and Hoxa-5 genes on the anterior/posterior axis in transgenic mice. Expressions of Hoxa-4 and Hoxa-5 genes were analyzed by in situ hybridization on sagittal frozen sections of 13-dpc embryos. Note that the anterior boundary of Hoxa-4 gene expression in transgenic (TG) embryos is on the first prevertebra (PV1) while in wild-type (WT) mice it is on the second prevertebra (PV2). The anterior boundary of Hoxa-5 gene expression in TG mice is on the third prevertebra (PV3) while in WT mice it is on the fourth prevertebra (PV4). drg = dorsal root ganglion.

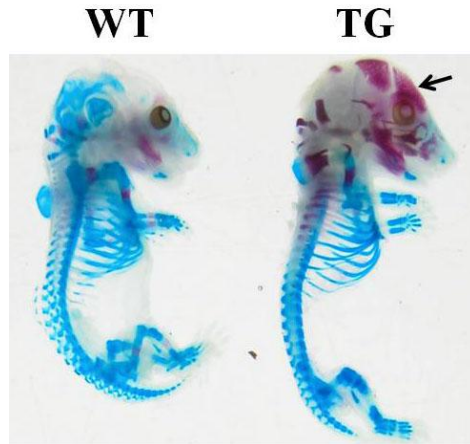


Figure 3.6 Advanced ossification in transgenic mice. Skeletons of 16.5 dpc embryos were stained with alizarin red and alcian blue. The ossification in transgenic (TG) mice (noted by arrow) occurs earlier than that in their wild-type (WT) littermates.

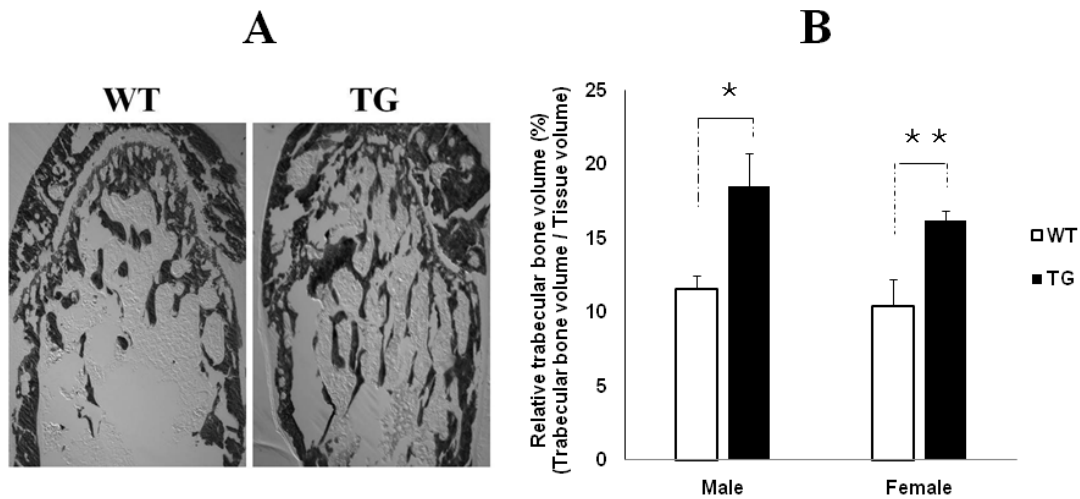


Figure 3.7 Increase of trabecular bone volume in transgenic mice. WT = wild-type, TG = transgenic. **A:** Von Kossa-stained femur bone sections from 3 month-old WT mice and their sex-matched TG littermates, showing TG mice have more trabecular bone than WT mice. **B:** Relative trabecular bone volume was significantly increased in femur bone of 3 month-old male and female transgenic mice. n=7 in both male and female WT group, n=8 in both male and female TG group. Values are presented as mean \pm SEM. The means between wild-type male group and transgenic male group, and the means between wild-type female group and transgenic female group differ at $P < 0.05$ (*) and $P < 0.01$ (**).

CHAPTER 4

GENERAL DISCUSSION AND CONCLUSIONS

4.1. General discussion

As described in Chapter 1, two highly related TGF- β superfamily members, myostatin and GDF11, have been recently identified as dominant factors that play essential roles in muscle growth and bone growth, respectively. However, myostatin and GDF11 are modulated by their antagonists, which may also play important roles in muscle growth or bone growth. Myostatin and GDF11 not only share a remarkably high homology, but also are regulated by similar mechanisms. It has been shown that myostatin and GDF11 could be suppressed by their own propeptides, suggesting myostatin propeptide and GDF11 propeptide may also play a role in regulating muscle growth and bone growth.

As shown in Chapter 2, a BMP-1/TLD-like metalloproteinases-resistant porcine myostatin propeptide not only effectively depressed myostatin activity *in vitro*, but also significantly promoted muscle growth *in vivo*. This suggests that the pig myostatin propeptide uses a similar regulation mechanism with that of other species to inhibit myostatin function, and the BMP-1/TLD-like metalloproteinases-resistant porcine myostatin propeptide may have application for improving muscle growth in pigs. However, production of recombinant protein from eukaryotic cells, like that in the present study, is highly costly. It probably is not cost effective to use eukaryotic cell-generated recombinant myostatin propeptide to enhance muscle growth in large meat animals, including pigs. A feasible strategy for boosting muscle growth in large animals is to over-express myostatin propeptide as a transgene under the control of a muscle-specific promoter in animals. Another strategy is to administer the large animals with recombinant

myostatin propeptide produced from the much cheaper bacterial expression system, since the absence of post-translational glycosylation of myostatin propeptide produced in prokaryotic cells does not affect the capacity of the propeptide to inhibit myostatin activity (Jiang et al., 2004).

As presented in Chapter 3, skeletal over-expression of GDF11 propeptide not only caused vertebral transformation but also enhances postnatal bone growth, suggesting GDF11 propeptide, as a GDF11 antagonist, also plays important role in bone growth. However, bone growth involves three dominant cellular events, including chondroblast-determined increase of bone size, osteoblast-mediated bone formation and osteoclast-responsible bone resorption. How GDF11 propeptide signal to modulate these three cellular events to regulate bone growth and what molecules are involved in this signaling pathway are still not clear. These issues should be further addressed in the future.

Although they share 90% identity in the amino acid sequence of their mature proteins, myostatin and GDF11 are believed to mainly play roles in muscle growth and skeleton formation, respectively, long after they were identified. However, recently accumulating evidence indicates that myostatin and GDF11 may play roles in both muscle growth and skeletal formation. Double knockouts of myostatin and GDF11 caused more serious skeletal defects than that in GDF11-deficient mice, suggesting myostatin also participates in skeletal patterning (McPherron et al., 2009). Myostatin also plays role in bone growth, since the myostatin-knockout mice have increased bone mineral content, bone mineral density and bone volume, and the myostatin propeptide transgenic mice have more bone mineral content and bone mineral density (Mitchel and Wall, 2007; Elkasrawy and Hamrick, 2010). For GDF11, it was able to block the differentiation of cultured myoblast cells into myotubes, and inhibit limb muscle development by reducing expressions of Pax3 and Myo D in chickens (Gamer et al., 2001; Souza et al., 2008).

Therefore, myostatin and GDF11, the two highly related molecules, appear to have overlapping functions in regulating both muscle growth and skeletal formation.

Although myostatin and GDF11 share high homology in their mature proteins, there is only 49% similarity in amino acid sequence between their propeptides (Ge et al., 2005). However, despite the low homology between them, myostatin propeptide and GDF11 propeptide can inhibit the activity of the mature protein of the other, in addition to blocking the activity of their own mature proteins, and their capacities to inhibit their own mature protein are very similar with that to inhibit the mature protein of the other (Thies et al., 2001; Ge et al., 2005). This cross inhibitory capacity of myostatin propeptide and GDF11 propeptide on the mature proteins of the other probably enable them to participate in regulations of extensive biological processes by down-regulating the functions of both myostatin and GDF11.

4.2. Conclusions

Research results from this project demonstrated significant effects of BMP-1/TLD-like metalloproteinases-resistant porcine myostatin propeptide on blocking myostatin activity and boosting muscle growth in both in vitro and in vivo models. The BMP-1/TLD-like metalloproteinases-resistant porcine myostatin propeptide was more effective in suppressing myostatin activity than the wild-type pig myostatin propeptide. Injection of the BMP-1/TLD-like metalloproteinases-resistant porcine myostatin propeptide into mice enhanced muscle growth by increasing muscle fiber size. These results suggest that pig myostatin propeptide may employ a similar mechanism as mouse myostatin propeptide to form a BMP-1/TLD-like metalloproteinases-activated complex to antagonize myostatin function. The mutated pig

myostatin propeptide is a potential ligand that could be used for promoting muscle growth in pigs. Further experiment with this protein in pigs is needed.

The function of GDF11 propeptide in regulating skeletal growth was studied in transgenic mice. Skeletal over-expression of GDF11 propeptide resulted in transformation of the seventh cervical vertebra into a thoracic vertebra. Expression of the GDF11 propeptide transgene appeared to start at the late embryonic stage. The transgene shifts of the anterior expression boundaries of Hoxa-4 and -5 genes from their normal prevertebra locations in 13 dpc embryos. Bone mineral content, bone mineral density and relative trabecular bone volume were significantly increased in transgenic mice. These results demonstrated that GDF11 not only controls vertebral formation by signaling through Hox genes, but also has effects on increasing bone mineral deposition and bone volume. The GDF11 propeptide transgenic mouse model is useful for further understanding of the functions of both GDF11 and its propeptide in regulation of bone formation and growth.

4.3. References

- Amthor H, Otto A, Vulin A, Rochat A, Dumonceaux J, Garcia L, Mouisel E, Hourdé C, Macharia R, Friedrichs M, Relaix F, Zammit PS, Matsakas A, Patel K, Partridge T. 2009. Muscle hypertrophy driven by myostatin blockade does not require stem/precursor-cell activity. *Proc Natl Acad Sci U S A* 106:7479-84.
- Andersson O, Reissmann E, Ibáñez CF. 2006. Growth differentiation factor 11 signals through the transforming growth factor-beta receptor ALK5 to regionalize the anterior-posterior axis. *EMBO Rep* 7:831-7.
- Bartoli M, Poupiot J, Vulin A, Fougerousse F, Arandel L, Daniele N, Roudaut C, Noulet F, Garcia L, Danos O, Richard I. 2007. AAV-mediated delivery of a mutated myostatin propeptide ameliorates calpain 3 but not alpha-sarcoglycan deficiency. *Gene Ther* 14:733-40.
- Bobbili NK, Kim YS, Dunn MA, Yang J, Ong A. 2008. Effects of maternal immunisation against myostatin on post-natal growth and skeletal muscle mass of offspring in mice. *Food Agric Immunol* 19:93-106.
- Boettiger D, Enomoto-Iwamoto M, Yoon H Y, Hofer U, Menko A S, Chiquet-Ehrismann R. 1995. Regulation of integrin $\alpha 5 \beta 1$ affinity during myogenic differentiation. *Dev. Biol* 169:

261–272.

Bogdanovich S, Krag TO, Barton ER, Morris LD, Whittemore LA, Ahima RS, Khurana TS.

2002. Functional improvement of dystrophic muscle by myostatin blockade. *Nature*

420:418-21.

Bogdanovich S, Perkins KJ, Krag TO, Whittemore LA, Khurana TS. 2005. Myostatin

propeptide-mediated amelioration of dystrophic pathophysiology. *FASEB J* 19:543–549.

Bo'ttinger, E P, Factor VM, Tsang MLS, Weatherbee JA, Kopp JB, Qian SW, Wakefield LM,

Roberts AB, Thorgeirsson SS, and Sporn MB. 1996. The recombinant proregion of

transforming growth factor β 1 (latency-associated peptide) inhibits active transforming

growth factor β 1 in transgenic mice. *Proc. Natl. Acad. Sci. USA* 93:5877–5882.

Brooke MH, Kaiser K K. 1970. Three 'myosin adenosine triphosphatase' systems: the nature of

their pH lability and sulphhydryl dependence. *Journal of Histochemistry and Cytochemistry*

18: 670-672.

Canalis E, Economides AN, Gazzerro E. 2003. Bone morphogenetic proteins, their antagonists,

and the skeleton. *Endocr Rev* 24:218-35.

Canalis E. 2009. Growth factor control of bone mass. *J Cell Biochem* 108:769-77.

Clop A, Marcq F, Takeda H, Pirottin D, Tordo X, Bibé B, Bouix J, Caiment F, Elsen JM,

- Eychenne F, Larzul C, Laville E, Meish F, Milenkovic D, Tobin J, Charlier C, Georges M. 2006. A mutation creating a potential illegitimate microRNA target site in the myostatin gene affects muscularity in sheep. *Nat Genet* 38:813-818.
- Copp DH, Cheney B. 1962. Calcitonin—a hormone from the parathyroid which lowers the calcium-level of the blood. *Nature* 193:381-2.
- Dacquin R, Starbuck M, Schinke T, Karsenty G. 2002. Mouse alpha1(I)-collagen promoter is the best known promoter to drive efficient Cre recombinase expression in osteoblast. *Dev Dyn* 224:245-51.
- Daluiski A, Engstrand T, Bahamonde ME, Gamer LW, Agius E, Stevenson SL, Cox K, Rosen V, Lyons KM. 2001. Bone morphogenetic protein-3 is a negative regulator of bone density. *Nat Genet* 27:84-8.
- David J D, See W M, Higginbotham C A. 1981. Fusion of chick embryo skeletal myoblasts: Role of calcium influx preceding membrane union. *Dev. Biol* 82: 297–307.
- Davis TA, Fiorotto ML, Burrin DG, Reeds PJ, Nguyen HV, Beckett PR, Vann RC, O'Connor PM. 2002. Stimulation of protein synthesis by both insulin and amino acids is unique to skeletal muscle in neonatal pigs. *Am J Physiol Endocrinol Metab* 282: E880–E890.
- Dayton WR, White ME. 2008. Cellular and molecular regulation of muscle growth and

- development in meat animals *J Anim Sci* 86(14 Suppl):E217-25.
- Dennler S, Itoh S, Vivien D, ten Dijke P, Huet S, Gauthier JM. 1998. Direct binding of smad3 and Smad4 to critical TGF beta-inducible elements in the promoter of human plasminogen activator inhibitor-type 1 gene. *EMBO J* 17:3091-100.
- Devlin RD, Du Z, Pereira RC, Kimble RB, Economides AN, Jorgetti V, Canalis E. 2003. Skeletal overexpression of noggin results in osteopenia and reduced bone formation. *Endocrinology*.144:1972-8.
- Ducy P, Zhang R, Geoffroy V, Ridall AL, Karsenty G. 1997. *Osf2/Cbfa1*: a transcriptional activator of osteoblast differentiation. *Cell* 89:747-54.
- Elkasrawy MN, Hamrick MW. 2010. Myostatin (GDF-8) as a key factor linking muscle mass and bone structure. *J Musculoskelet Neuronal Interact* 10:56-63.
- Enomoto H, Enomoto-Iwamoto M, Iwamoto M, Nomura S, Himeno M, Kitamura Y, Kishimoto T, Komori T. 2000. *Cbfa1* is a positive regulatory factor in chondrocyte maturation. *J Biol Chem* 275:8695-702.
- Esquela AF, Lee SJ. 2003. Regulation of metanephric kidney development by growth/differentiation factor 11. *Dev Biol* 257:356-70
- Essalmani R, Zaid A, Marcinkiewicz J, Chamberland A, Pasquato A, Seidah NG, Prat A. 2008.

- In vivo functions of the proprotein convertase PC5/6 during mouse development: Gdf11 is a likely substrate. *Proc Natl Acad Sci U S A* 105:5750-5.
- Favier B, Dollé P. 1997. Developmental functions of mammalian Hox genes. *Mol Hum Reprod* 3:115-31.
- Galis F. 1999. Why do almost all mammals have seven cervical vertebrae? Developmental constraints, Hox genes, and cancer. *J Exp Zool* 285:19-26.
- Gamer LW, Wolfman NM, Celeste AJ, Hattersley G, Hewick R, Rosen V. 1999. A novel BMP expressed in developing mouse limb, spinal cord, and tail bud is a potent mesoderm inducer in *Xenopus* embryos. *Dev Biol* 208:222-32.
- Gamer LW, Cox KA, Small C, Rosen V. 2001. Gdf11 is a negative regulator of chondrogenesis and myogenesis in the developing chick limb. *Dev Biol* 15;229:407-20.
- Gauthier GF. 1969. On the relationship of ultrastructural and cytochemical features to color in mammalian skeletal muscle. *Zeitschrift fur Zellforschung* 95: 462-482.
- Gazzerro E, Pereira RC, Jorgetti V, Olson S, Economides AN, Canalis E. 2005. Skeletal overexpression of gremlin impairs bone formation and causes osteopenia. *Endocrinology* 146:655-65.
- Ge G, Hopkins DR, Ho WB, Greenspan DS. 2005. GDF11 forms a bone morphogenetic protein

activated latent complex that can modulate nerve growth factor-induced differentiation of PC12 cells. *Mol Cell Biol* 25:5846-58.

Grobet L, Martin LJ, Poncelet D, Pirottin D, Brouwers B, Riquet J, Schoeberlein A, Dunner S, Méniéssier F, Massabanda J, Fries R, Hanset R, Georges M. 1997. A deletion in the bovine myostatin gene causes the double-muscled phenotype in cattle. *Nature Genet* 17:71–74.

Haidet AM, Rizo L, Handy C, Umapathi P, Eagle A, Shilling C, Boue D, Martin PT, Sahenk Z, Mendell JR, Kaspar BK. 2008. Longterm enhancement of skeletal muscle mass and strength by single gene administration of myostatin inhibitors. *Proc Natl Acad Sci USA* 105:4318–4322.

Hess K, Ushmorov A, Fiedler J, Brenner RE, Wirth T. 2009. TNFalpha promotes osteogenic differentiation of human mesenchymal stem cells by triggering the NF-kappaB signaling pathway. *Bone* 45:367-76.

Hill JJ, Davies MV, Pearson AA, Wang JH, Hewick RM, Wolfman NM, Qiu Y. 2002. The myostatin propeptide and the follistatin-related gene are inhibitory binding proteins of myostatin in normal serum. *J Biol Chem* 277:40735-41.

Horan GS, Wu K, Wolgemuth DJ, Behringer RR. 1994. Homeotic transformation of cervical vertebrae in *Hoxa-4* mutant mice. *Proc Natl Acad Sci U S A* 91:12644-12648.

Hume EM, Lucas NS, Smith HH. 1927. On the Absorption of Vitamin D from the Skin.

Biochem J 21: 362–367.

Iemura S, Yamamoto TS, Takagi C, Uchiyama H, Natsume T, Shimasaki S, Sugino H, Ueno N.

1998. Direct binding of follistatin to a complex of bone-morphogenetic protein and its receptor inhibits ventral and epidermal cell fates in early *Xenopus* embryo. Proc Natl Acad Sci U S A 95:9337-42.

Jeannotte L, Lemieux M, Charron J, Poirier F, Robertson EJ. 1993. Specification of axial identity

in the mouse: role of the *Hoxa-5* (*Hox1.3*) gene. Genes Dev 7:2085-2096.

Ji M, Zhang Q, Ye J, Wang X, Yang W, Zhu D. 2008. Myostatin induces p300 degradation to

silence cyclin D1 expression through the PI3K/PTEN/Akt pathway. Cell Signal 20:1452-8.

Jiang MS, Liang LF, Wang S, Ratovitski T, Holmstrom J, Barker C, Stotish R. 2004.

Characterization and identification of the inhibitory domain of GDF-8 propeptide. Biochem Biophys Res Commun 315:525-31.

Kambadur R, Sharma M, Smith TPL, Bass JJ. 1997. Mutations in myostatin (GDF8) in double-

muscled Belgian Blue and Piedmontese cattle. Genome Res 7:910–915.

Kawazoe Y, Sekimoto T, Araki M, Takagi K, Araki K, Yamamura K. 2002. Region-specific

gastrointestinal Hox code during murine embryonal gut development. Dev Growth Differ

44:77-84.

Kim YS, Bobbili NK, Paek KS, Jin HJ. 2006. Production of a monoclonal anti-myostatin antibody and the effects of in ovo administration of the antibody on posthatch broiler growth and muscle mass. *Poult Sci* 85:1062-71.

Kim YS, Bobbili NK, Lee YK, Jin HJ, Dunn MA. 2007. Production of a polyclonal anti-myostatin antibody and the effects of in ovo administration of the antibody on posthatch broiler growth and muscle mass. *Poult Sci* 86:1196-205.

Klont RE, Brocks L, Eikelenboom G. 1998. Muscle fibre type and meat quality. *Meat Science* 49: S219–S229.

Knudsen K A. 1985. The calcium-dependent myoblast adhesion that precedes cell fusion is mediated by glycoproteins. *J. Cell Biol* 101: 891–897.

Komori T, Yagi H, Nomura S, Yamaguchi A, Sasaki K, Deguchi K, Shimizu Y, Bronson RT, Gao YH, Inada M, Sato M, Okamoto R, Kitamura Y, Yoshiki S, Kishimoto T. 1997. Targeted disruption of *Cbfa1* results in a complete lack of bone formation owing to maturational arrest of osteoblasts. *Cell* 89:755-64.

Kugimiya F, Kawaguchi H, Kamekura S, Chikuda H, Ohba S, Yano F, Ogata N, Katagiri T, Harada Y, Azuma Y, Nakamura K, Chung UI. 2005. Involvement of endogenous bone

- morphogenetic protein (BMP) 2 and BMP6 in bone formation. *J Biol Chem* 280:35704-35712.
- Laemmli UK. 1970. Cleavage of structural proteins during the assembly of the head of bacteriophage T4. *Nature* 227: 680-5.
- Langley B, Thomas M, Bishop A, Sharma M, Gilmour S, Kambadur R. 2002. Myostatin inhibits myoblast differentiation by down-regulating MyoD expression. *J Biol Chem* 277:49831-49840.
- Langman CB. 2000. New developments in calcium and vitamin D metabolism. *Curr Opin Pediatr* 12:135-139.
- Lee S-J, McPherron AC. 2001. Regulation of myostatin activity and muscle growth. *Proc Natl Acad Sci USA* 98:9306-9311.
- Lee S-J. 2004. Regulation of muscle mass by myostatin. *Annu Rev Cell Dev Biol* 20: 61-86.
- Lee S-J, Reed LA, Davies MV, Girgenrath S, Goad ME, Tomkinson KN, Wright JF, Barker C, Ehrmantraut G, Holmstrom J, Trowell B, Gertz B, Jiang MS, Sebald SM, Matzuk M, Li E, Lee S-J. 2007. Quadrupling muscle mass in mice by targeting TGF-beta signaling pathways. *PLoS One* 2:e789.
- Lee S-J. 2008. Genetic analysis of the role of proteolysis in the activation of latent myostatin.

- Li Z, Cao B, Zhao B, Yang X, Fan MZ, Yang J. 2009. Decreased expression of calpain and calpastatin mRNA during development is highly correlated with muscle protein accumulation in neonatal pigs. *Comp Biochem Physiol A Mol Integr Physiol* 152:498-503.
- Liang LF, Quattlebaum E, Stotish RL, Wolfman NM. 2005. Regulation of muscle growth by multiple ligands signaling through activin type II receptors. *Proc Natl Acad Sci U S A* 102:18117-22.
- Luff RA, Goldspink G. 1970. Total number of fibers in muscles of several strains of mice. *J Anim Sci* 30: 891-893.
- Makhoul RG, Machleder HI. 1992. Developmental anomalies at the thoracic outlet: an analysis of 200 consecutive cases. *J Vasc Surg* 16:534-542.
- Manak JR, Scott MP. 1994. A class act: conservation of homeodomain protein functions. *Dev Suppl* 1994: 61-77.
- Mark M, Rijli FM, Chambon P. 1997. Homeobox genes in embryogenesis and pathogenesis. *Pediatr Res* 42:421-429.
- McCroskery S, Thomas M, Maxwell L, Sharma M, Kambadur R. 2003. Myostatin negatively regulates satellite cell activation and self-renewal. *J Cell Biol* 162:1135-47.

- McFarlane C, Plummer E, Thomas M, Hennebry A, Ashby M, Ling N, Smith H, Sharma M, Kambadur R. 2006. Myostatin induces cachexia by activating the ubiquitin proteolytic system through an NF-kappaB-independent, FoxO1-dependent mechanism. *J Cell Physiol* 209:501-14.
- McPherron AC, Lawler AM, Lee S-J. 1997. Regulation of skeletal muscle mass in mice by a new TGF- β superfamily member. *Nature* 387:83-90.
- McPherron AC, Lee S-J. 1997. Double muscling in cattle due to mutations in the myostatin gene. *Proc Natl Acad Sci USA* 94:12457-12461.
- McPherron AC, Lawler AM, Lee SJ. 1999. Regulation of anterior/posterior patterning of the axial skeleton by growth/differentiation factor 11. *Nat Genet* 22:260-4
- McPherron AC, Huynh TV, Lee SJ. 2009. Redundancy of myostatin and growth/differentiation factor 11 function. *BMC Dev Biol* 9:24.
- Mitchell AD, Wall RJ. 2007. In vivo evaluation of changes in body composition of transgenic mice expressing the myostatin pro domain using dual energy X-ray absorptiometry. *Growth Dev Aging* 70: 25-37.
- Mosher DS, Quignon P, Bustamante CD, Sutter NB, Mellersh CS, Parker HG, Ostrander EA. 2007. A mutation in the myostatin gene increases muscle mass and enhances racing

- performance in heterozygote dogs. *PLoS Genet* 3:0779-0786.
- Nakashima M, Toyono T, Akamine A, Joyner A. 1999. Expression of growth/differentiation factor 11, a new member of the BMP/TGFbeta superfamily during mouse embryogenesis. *Mech Dev* 80:185-9.
- O'Brien SP, Seipel K, Medley QG, Bronson R, Segal R, Streuli M. 2000. Skeletal muscle deformity and neuronal disorder in Trio exchange factor-deficient mouse embryos. *Proc Natl Acad Sci U S A* 97:12074-8.
- Oh SP, Li E. 1997. The signaling pathway mediated by the type IIB activin receptor controls axial patterning and lateral asymmetry in the mouse. *Genes Dev* 11:1812-26.
- Oh SP, Yeo CY, Lee Y, Schrewe H, Whitman M, Li E. 2002. Activin type IIA and IIB receptors mediate Gdf11 signaling in axial vertebral patterning. *Genes Dev* 16:2749-54.
- Oksbjerg N, Gondret F, Vestergaard M. 2004. Basic principles of muscle development and growth in meat-producing mammals as affected by the insulin-like growth factor (IGF) system. *Domest Anim Endocrinol* 27:219-40.
- Perry R, Rudnick M. 2000. Molecular mechanisms regulating myogenic determination and differentiation. *Front Biosci* 5:D750-67.
- Peter JB, Bainard RJ, Edgerton VR, Gillespie CA, Stempel KE. 1972. Metabolic profiles of three

- fiber types of skeletal muscle in guinea pigs and rabbits. *Biochemistry* 11: 2627-2633.
- Pirottin D, Grobet L, Adamantidis A, Farnir F, Herens C, Daa Schrøder H, Georges M. 2005. Transgenic engineering of male-specific muscular hypertrophy. *Proc Natl Acad Sci U S A*. 102:6413-8.
- Rebbapragada A, Benchabane H, Wrana JL, Celeste AJ, Attisano L. 2003. Myostatin signals through a transforming growth factor beta-like signaling pathway to block adipogenesis. *Mol Cell Biol* 23:7230-42.
- Reisz-Porszasz S, Bhasin S, Artaza JN, Shen R, Sinha-Hikim I, Hogue A, Fielder TJ, Gonzalez-Cadavid NF. 2003. Lower skeletal muscle mass in male transgenic mice with muscle-specific overexpression of myostatin. *Am J Physiol Endocrinol Metab* 285:E876-88.
- Rios R, Carneiro I, Arce VM, Devesa J. 2002. Myostatin is an inhibitor of myogenic differentiation. *Am J Physiol Cell Physiol* 282:C993–C999.
- Rommel C, Bodine SC, Clarke BA, Rossman R, Nunez L, Stitt TN, Yancopoulos GD, and Glass DJ. 2001. Mediation of IGF-1-induced skeletal myotube hypertrophy by PI3K/Akt/mTOR and PI3K/Akt/GSK3 pathways. *Nat Cell Biol* 3: 1009–1013.
- Roos DB. 1996. Historical perspectives and anatomic considerations. Thoracic outlet syndrome. *Semin Thorac Cardiovasc Surg* 8:183-189.

- Rossert J, Eberspaecher H, de Crombrughe B. 1995. Separate cis-acting DNA elements of the mouse pro-alpha 1(I) collagen promoter direct expression of reporter genes to different type I collagen-producing cells in transgenic mice. *J Cell Biol* 129:1421-32.
- Sacheck JM, Ohtsuka A, McLary SC, Goldberg AL. 2004. IGF-I stimulates muscle growth by suppressing protein breakdown and expression of atrophy-related ubiquitin ligases, atrogin-1 and MuRF1. *Am J Physiol Endocrinol Metab* 287(4):E591-601.
- Sartori R, Milan G, Patron M, Mammucari C, Blaauw B, Abraham R, Sandri M. 2009. Smad2 and 3 transcription factors control muscle mass in adulthood. *Am J Physiol Cell Physiol* 296:C1248-57.
- Schuelke M, Wagner KR, Stolz LE, Hübner C, Riebel T, Kömen W, Braun T, Tobin JF, Lee SJ. 2004. Myostatin mutation associated with gross muscle hypertrophy in a child. *N Engl J Med* 350:2682-8.
- Schumacher R, Mai A, Gutjahr P. 1992. Association of rib anomalies and malignancy in childhood. *Eur J Pediatr* 151:432-434.
- Seale P, Rudnicki MA. 2000. A new look at the origin, function, and "stem-cell" status of muscle satellite cells. *Dev Biol* 218:115-24.
- Shea CM, Edgar CM, Einhorn TA, Gerstenfeld LC. 2003. BMP treatment of C3H10T1/2

mesenchymal stem cells induces both chondrogenesis and osteogenesis. *J Cell Biochem* 90:1112-27.

Souza TA, Chen X, Guo Y, Sava P, Zhang J, Hill JJ, Yaworsky PJ, Qiu Y. 2008. Proteomic identification and functional validation of activins and bone morphogenetic protein 11 as candidate novel muscle mass regulators. *Mol Endocrinol* 22:2689-702.

Steinert AF, Proffen B, Kunz M, Hendrich C, Ghivizzani SC, Nöth U, Rethwilm A, Eulert J, Evans CH. 2009. Hypertrophy is induced during the in vitro chondrogenic differentiation of human mesenchymal stem cells by bone morphogenetic protein-2 and bone morphogenetic protein-4 gene transfer. *Arthritis Res Ther* 11:R148.

Suda T, Udagawa N, Nakamura I, Miyaura C, Takahashi N. 1995. Modulation of osteoclast differentiation by local factors. *Bone* 17(2 Suppl): 87S–91S.

Suryawan A, Frank JW, Nguyen HV, Davis TA. 2006. Expression of the TGF-beta family of ligands is developmentally regulated in skeletal muscle of neonatal rats. *Pediatric Research* 59: 175-9.

Suzawa M, Takeuchi Y, Fukumoto S, Kato S, Ueno N, Miyazono K, Matsumoto T, Fujita T. 1999. Extracellular matrix-associated bone morphogenetic proteins are essential for differentiation of murine osteoblastic cells in vitro. *Endocrinology* 140:2125-33.

- Takahara Y, Tomotsune D, Shirai M, Katoh-Fukui Y, Nishii K, Motaleb MA, Nomura M, Tsuchiya R, Fujita Y, Shibata Y, Higashinakagawa T, Shimada K. 1997. Targeted disruption of the mouse homologue of the *Drosophila* polyhomeotic gene leads to altered anteroposterior patterning and neural crest defects. *Development* 124:3673-3682.
- Taylor WE, Bhasin S, Artaza J, Byhower F, Azam M, Willard DH Jr, Kull FC Jr, Gonzalez-Cadavid N. 2001. Myostatin inhibits cell proliferation and protein synthesis in C2C12 muscle cells. *Am J Physiol Endocrinol Metab* 280:E221–E228.
- Thayer M J, Tapscott S J, Davis R L, Wright W E, Lassar A B, Weintraub H. 1989. Positive autoregulation of the myogenic determination gene *MyoD1*. *Cell* 58:241-8.
- Thies RS, Chen T, Davies MV, Tomkinson KN, Pearson AA, Shakey QA, Wolfman NM. 2001. GDF-8 propeptide binds to GDF-8 and antagonizes biological activity by inhibiting GDF-8 receptor binding. *Growth Factors* 18: 251-9.
- Thomas M, Langley B, Berry C, Sharma M, Kirk S, Bass J, Kambadur R. 2000. Myostatin, a negative regulator of muscle growth, functions by inhibiting myoblast proliferation. *J Biol Chem* 275:40235–40243.
- Tordoff MG, Hughes RL, Pilchak DM. 1998. Calcium intake by rats: influence of parathyroid hormone, calcitonin, and 1,25-dihydroxyvitamin D. *Am J Physiol* 274(1 Pt 2): R214-31.

Tscheudschilsuren G, Bosserhoff AK, Schlegel J, Vollmer D, Anton A, Alt V, Schnettler R,

Brandt J, Proetzel G. 2006. Regulation of mesenchymal stem cell and chondrocyte differentiation by MIA. *Exp Cell Res* 312:63-72.

Urschitz J, Kawasumi M, Owens J, Morozumi K, Yamashiro H, Stoytchev I, Marh J, Dee JA,

Kawamoto K, Coates CJ, Kaminski JM, Pelczar P, Yanagimachi R, Moisyadi S. 2010.

Helper-independent piggyBac plasmids for gene delivery approaches: Strategies for avoiding potential genotoxic effects. *Proc Natl Acad Sci U S A* doi:

10.1073/pnas.1003674107 (published online before print)

Veldman GM, Widom A, Wright JF, Wudyka S, Zhao L, Wolfman NM. 2003. Inhibition of

myostatin in adult mice increases skeletal muscle mass and strength. *Biochem Biophys Res Commun* 300:965-71.

Wan M, Cao X. 2005. BMP signaling in skeletal development. *Biochem Biophys Res Commun*

18;328:651-7.

Wegner J, Albrecht E, Fiedler I, Teuscher F, Papstein HJ, Ender K. 2000. Growth- and breed-

related. *J Anim Sci* 78: 1485- 496.

Weintraub H, Tapscott S J, Davis R L, Thayer M J, Adam M A, Lassar A B, Miller D. 1989.

Activation of muscle-specific genes in pigment, nerve, fat, liver, and fibroblast cell lines by

forced expression of MyoD. *Proc. Natl. Acad. Sci. USA* 86: 5434–5438.

Weintraub H, Davis R, Tapscott S, Thayer M, Krause M, Benezra R, Blackwell T, Turner D,

Rupp R, Hollenberg S. 1991. The myoD gene family: nodal point during specification of the muscle cell lineage. *Science* 251 (4995):761–6.

Wellik DM. 2007. Hox patterning of the vertebrate axial skeleton. *Dev Dyn* 236:2454–63.

Whittemore LA, Song K, Li X, Aghajanian J, Davies M, Girgenrath S, Hill JJ, Jalenak M, Kelley

P, Knight A, Maylor R, O'Hara D, Pearson A, Quazi A, Ryerson S, Tan XY, Tomkinson

KN, Wolfman NM, McPherron AC, Pappano WN, Davies MV, Song K, Tomkinson KN,

Wright JF, Zhao L, Sebald SM, Greenspan DS, Lee SJ. 2003. Activation of latent myostatin

by the BMP-1/tolloid family of metalloproteinases. *Proc Natl Acad Sci USA* 100:15842–

15846.

Wolfman, N. M., A. C. McPherron, W. N. Pappano, M. V. Davies, K. Song, K. N. Tomkinson, J.

F. Wright, L. Zhao, S. M. Sebald, D. S. Greenspan, and S.-J. Lee. 2003. Activation of latent

myostatin by the BMP-1/tolloid family of metalloproteinases. *Proc. Natl. Acad. Sci. USA*

100:15842–15846.

Wu Z, Li Z, Yang J. 2008. Transient transgene transmission to piglets by intrauterine

insemination of spermatozoa incubated with DNA fragments. *Mol Reprod Dev* 75: 26–32.

Yagami-Hiromasa T, Sato T, Kurisaki T, Kamijo K, Nabeshima Y -I, Fujisawa-Sehara A. 1995.

A metalloprotease-disintegrin participating in myoblast fusion. *Nature* 377: 652–656.

Yang J, Ratovitski T, Brady JP, Solomon MB, Wells KD, Wall RJ. 2001. Expression of

myostatin pro domain results in muscular transgenic mice. *Mol Reprod Dev* 60:51-61

Yang J, Zhao B. 2006. Postnatal expression of myostatin propeptide cDNA maintained high

muscle growth and normal adipose tissue mass in transgenic mice fed a high-fat diet. *Mol*

Reprod Dev 73: 462-9.

Yang W, Zhang Y, Li Y, Wu Z, Zhu D. 2006. Myostatin induces cyclin D1 degradation to cause

cell cycle arrest through a phosphatidylinositol 3-kinase/AKT/GSK-3 beta pathway and is

antagonized by insulin-like growth factor 1. *J Biol Chem* 282:3799-808.

Zhu MJ, Ford SP, Nathanielsz PW, Du M. 2004. Effect of maternal nutrient restriction in sheep

on the development of fetal skeletal muscle. *Biol Reprod* 71:1968-73.

Zimmers TA, Davies MV, Koniaris LG, Haynes P, Esquela AF, et al. 2002. Induction of

cachexia in mice by systemically administered myostatin. *Science* 296:1486–1488.

4.4. Appendices

4.4.1. Appendix A: The raw data of Table 2.1.

Carcass and muscle weight (in g) of male mice injected with PBS (n=16)

Carcass	Triceps	Pectoralis	Longissimus	Semitendinosus	Gastrocnemius	Triceps
7.40	0.07	0.13	0.17	0.14	0.11	0.08
7.90	0.10	0.12	0.19	0.15	0.11	0.06
8.10	0.07	0.11	0.20	0.14	0.09	0.09
7.60	0.08	0.09	0.18	0.11	0.14	0.07
7.79	0.07	0.10	0.19	0.12	0.10	0.09
8.40	0.09	0.13	0.15	0.11	0.10	0.07
7.80	0.08	0.10	0.17	0.10	0.10	0.06
7.90	0.08	0.13	0.19	0.11	0.13	0.07
7.50	0.07	0.10	0.21	0.12	0.10	0.08
8.14	0.09	0.12	0.26	0.12	0.13	0.06
7.80	0.08	0.12	0.11	0.12	0.11	0.07
8.50	0.09	0.15	0.24	0.13	0.12	0.07
7.33	0.07	0.09	0.21	0.10	0.13	0.07
7.55	0.08	0.13	0.20	0.11	0.09	0.07
8.00	0.10	0.12	0.18	0.09	0.11	0.10
7.20	0.10	0.10	0.19	0.12	0.11	0.08

Carcass and muscle weight (in g) of male mice injected with mutated propeptide (n=9)

Carcass	Triceps	Pectoralis	Longissimus	Semitendinosus	Gastrocnemius	Triceps
8.50	0.08	0.13	0.17	0.12	0.12	0.07
9.85	0.09	0.12	0.21	0.12	0.16	0.10
9.35	0.13	0.13	0.18	0.15	0.15	0.08
9.56	0.11	0.13	0.19	0.14	0.13	0.07
9.08	0.07	0.13	0.23	0.15	0.14	0.08
9.82	0.11	0.16	0.32	0.17	0.14	0.08
9.54	0.12	0.15	0.25	0.14	0.14	0.09
8.71	0.09	0.16	0.24	0.13	0.15	0.10
9.48	0.12	0.16	0.27	0.13	0.12	0.09

Carcass and muscle weight (in g) of female mice injected with PBS (n=7)

Carcass	Triceps	Pectoralis	Longissimus	Semitendinosus	Gastrocnemius	Triceps
6.90	0.08	0.08	0.09	0.09	0.08	0.07
6.00	0.07	0.06	0.17	0.09	0.10	0.05
6.27	0.08	0.09	0.16	0.10	0.11	0.06
6.10	0.07	0.07	0.10	0.10	0.10	0.06
6.09	0.06	0.07	0.15	0.10	0.12	0.05
5.93	0.06	0.08	0.15	0.10	0.11	0.06
6.23	0.07	0.07	0.14	0.08	0.09	0.06

Carcass and muscle weight (in g) of female mice injected with mutated propeptide (n=6)

Carcass	Triceps	Pectoralis	Longissimus	Semitendinosus	Gastrocnemius	Triceps
7.38	0.07	0.08	0.12	0.09	0.12	0.06
7.40	0.08	0.06	0.14	0.11	0.10	0.07
7.10	0.08	0.10	0.16	0.13	0.13	0.08
7.27	0.08	0.09	0.20	0.11	0.11	0.08
7.54	0.10	0.09	0.18	0.12	0.09	0.06
7.22	0.10	0.10	0.15	0.11	0.14	0.07

4.4.2. Appendix B: The raw data of Figure 2.3.

Firefly luciferase activity and renilla luciferase activity in A204 cells at 6h after addition with 20ng/ml of myostatin and different concentrations of mutated pig myostatin propeptides (n=6 at each concentration of mutated propeptide).

Mutated propeptide (ng/ml)	0	1	10	50	100	500	1000	No myostatin
Firefly	143006	227757	80841	129815	12802	4859	1840	1850
Firefly	96847	99419	110010	96003	11544	2767	1727	1637
Firefly	63875	86383	72387	93047	10584	1678	2056	1805
Firefly	154693	92262	169248	55928	12324	2332	2077	5059
Firefly	62776	43973	94415	52216	8666	923	1108	1079
Firefly	167013	58786	60434	74088	6288	1658	1425	x
Renilla	4086	7095	3038	4517	3494	2816	1914	1518
Renilla	3537	3290	3199	3038	3185	2240	5148	1392
Renilla	1725	3135	2197	2436	2297	2210	3670	1561
Renilla	6266	2227	3670	2676	2117	2207	3116	2057
Renilla	2478	1455	2773	1867	2035	1925	1034	1124
Renilla	4112	1464	1768	2795	2261	1962	2052	x

Firefly luciferase activity and renilla luciferase activity in A204 cells at 6h after addition with 20ng/ml of myostatin and different concentrations of wild-type pig myostatin propeptides (n=6 at each concentration of wild-type propeptide).

Wild-type propeptide (ng/ml)	0	1	10	50	100	500	1000
Firefly	129632	79616	154698	58623	11598	3562	985
Firefly	140533	153499	98652	45623	6853	3548	1325
Firefly	90444	153691	76962	86521	9812	2987	2451
Firefly	101625	72365	83606	124568	7821	1783	2658
Firefly	79824	97880	74562	56384	6523	3014	1983
Firefly	139882	57246	45982	74562	10478	1254	1235
Renilla	4285	2548	4218	3193	2042	3527	527
Renilla	3866	4135	2624	1691	1084	5458	1380
Renilla	2651	5696	1914	3186	1982	7861	1857
Renilla	3852	2595	2971	5160	1574	1592	2606
Renilla	3073	3667	2475	2005	1093	5382	931
Renilla	4827	2313	1352	2496	1370	2787	433

4.4.3. Appendix C: The raw data of Figure 2.4.

Firefly luciferase activity and renilla luciferase activity in A204 cells at 6h, 24h and 48h after addition with 20ng/ml of myostatin and 100ng/ml of wild-type or mutated pig myostatin propeptides (My=Myostatin; Mu=Mutated pig myostatin propeptide; WT=Wild-type pig myostatin propeptide; n=6 at each co-incubation time).

Co-incubation time	6h	6h	6h	24h	24h	24h	48h	48h	48h
Firefly	112365	9865	15684	85321	16815	29862	45689	20587	41283
Firefly	133422	13245	19862	95621	13269	27320	56721	20978	26136
Firefly	76151	15634	12365	65287	12868	21457	40125	21458	39687
Firefly	93953	23145	14523	71365	13958	38786	34156	14325	39860
Firefly	166847	19564	20135	82341	18961	28756	54268	16897	20358
Firefly	115687	10655	19821	79531	26386	27561	56237	22780	23598
Renilla	3574	2771	2237	3022	2555	3190	2361	2801	3287
Renilla	3785	2328	2912	4319	2349	2774	2410	2893	1956
Renilla	1898	5264	3388	2658	1523	1842	2654	2636	3713
Renilla	3594	5446	4873	2449	3910	4066	2766	2449	2797
Renilla	6852	2856	3430	3248	4060	4186	2805	2600	1620
Renilla	3262	3088	3657	3392	4010	3699	3058	2805	1851
	My	My+Mu	My+WT	My	My+Mu	My+WT	My	My+Mu	My+WT

4.4.4. Appendix D: The raw data of Figure 2.5.

Body weight (in g) of male mice after injection with PBS (n=16)

11 d-old	18 d-old	25 d-old	32 d-old	39 d-old	46 d-old	53 d-old	57 d-old
6.40	7.80	11.70	17.10	20.00	20.50	20.80	20.80
6.30	9.00	12.30	18.00	19.50	20.80	23.40	21.40
6.10	7.40	10.90	14.90	19.50	23.10	21.10	24.20
5.90	7.10	10.70	15.20	16.80	18.20	19.60	20.80
5.90	6.60	11.30	17.20	19.20	18.00	21.80	22.80
6.40	8.10	12.00	17.30	20.10	19.10	19.90	19.90
5.90	7.20	10.80	16.90	19.20	21.50	21.10	20.70
6.30	8.10	12.20	19.50	17.00	17.10	21.30	20.80
6.30	6.70	12.40	19.90	17.00	21.20	21.70	22.10
5.70	7.50	10.80	15.80	20.40	20.40	20.00	23.20
6.10	7.50	10.90	14.70	20.00	20.20	19.80	22.80
5.90	9.10	9.80	14.20	17.80	22.30	19.50	22.90
6.20	7.30	9.80	14.40	20.30	21.00	19.80	20.80
5.60	8.40	10.80	15.20	21.00	17.80	21.90	20.40
5.70	7.40	10.60	15.10	16.10	21.50	23.40	21.30
6.10	6.90	11.00	15.20	17.40	18.60	20.90	21.40

Body weight (in g) of male mice after injection with mutated pig myostatin propeptide (n=9)

11 d-old	18 d-old	25 d-old	32 d-old	39 d-old	46 d-old	53 d-old	57 d-old
6.20	8.70	12.70	18.40	20.70	24.20	22.90	23.80
6.50	8.80	12.20	17.20	21.90	21.40	22.10	25.40
5.80	7.00	11.70	17.30	20.10	24.50	24.90	25.80
6.10	9.00	11.90	18.40	22.00	23.20	21.00	22.20
5.80	7.50	12.70	18.70	22.50	22.40	24.80	23.00
6.10	8.70	13.80	19.60	21.20	22.20	25.00	21.90
6.00	8.30	12.30	20.60	21.60	24.10	23.80	23.30
6.30	7.80	13.40	19.50	21.40	21.00	24.00	22.60
5.80	7.60	14.30	18.60	20.60	23.10	22.70	24.10

Body weight (in g) of female mice after injection with PBS (n=7)

11 d-old	18 d-old	25 d-old	32 d-old	39 d-old	46 d-old	53 d-old	57 d-old
6.50	8.10	10.40	14.70	15.90	19.40	17.00	17.50
5.60	7.00	9.80	14.10	14.30	15.80	17.80	18.40
6.30	7.70	11.80	12.90	15.70	16.70	15.70	18.40
5.70	7.40	11.10	13.70	14.50	16.80	17.20	17.80
5.60	6.70	9.60	12.50	17.00	16.00	16.80	16.50
6.20	7.90	11.10	12.70	14.80	18.80	16.80	18.30
5.70	6.80	9.60	14.90	17.00	16.00	19.20	19.90

Body weight (in g) of female mice after injection with mutated pig myostatin propeptide (n=6)

11 d-old	18 d-old	25 d-old	32 d-old	39 d-old	46 d-old	53 d-old	57 d-old
6.30	8.90	12.00	16.90	18.70	19.70	19.00	19.60
6.00	7.90	11.60	14.50	16.40	18.90	21.10	21.30
6.10	8.40	11.40	14.30	16.50	21.27	19.60	19.10
6.20	8.40	13.10	14.90	18.50	19.30	20.80	21.60
5.70	7.20	12.20	15.40	16.70	17.10	18.40	19.40
5.90	8.20	11.60	16.30	17.60	17.50	19.50	19.80

4.4.5. Appendix E: The raw data of Figure 2.6.

The area and fiber number of 16 randomly selected spots in cross section of Longissimus muscle of 4 randomly selected male mice injected with mutated pig myostatin propeptide.

	Animal 1		Animal 2		Animal 3		Animal 4	
Spot	Area (μm^2)	Fiber number	Area (μm^2)	Fiber number	Area (μm^2)	Fiber number	Area (μm^2)	Fiber number
1	5698	30	1985	12	5752	31	2369	15
2	3615	20	2672	13	4047	25	4567	23
3	2201	14	2687	14	6120	28	1756	9
4	4089	20	2858	16	3903	27	2547	13
5	3698	16	2310	17	4332	22	4017	24
6	4000	16	4073	25	1712	12	4210	26
7	2980	15	5468	34	1056	9	3547	15
8	6400	33	1560	9	5929	25	3987	17
9	3621	17	2889	15	3086	20	3297	19
10	3012	17	4300	23	2022	14	2985	18
11	3139	15	2431	13	2271	12	1847	12
12	3874	18	3800	19	3192	20	1762	11
13	3241	17	4012	19	3404	27	4012	20
14	3720	20	3265	17	2346	14	3954	13
15	3412	19	3802	19	5308	28	1765	10
16	2600	15	1012	15	2033	13	3895	27

The area and fiber number of 16 randomly selected spots in cross section of Longissimus muscle
of 4 randomly selected male mice injected with PBS.

	Animal 1		Animal 2		Animal 3		Animal 4	
Spot	Area (μm^2)	Fiber number	Area (μm^2)	Fiber number	Area (μm^2)	Fiber number	Area (μm^2)	Fiber number
1	2820	19	2959	17	1890	12	1573	10
2	2560	21	805	9	2150	16	1875	15
3	4569	17	1865	12	1909	16	2011	17
4	4645	21	2265	24	3124	25	2641	20
5	4501	28	2100	19	2230	13	2134	23
6	1550	17	1479	15	7520	31	812	8
7	1952	17	2503	15	3857	27	1852	12
8	1608	10	2487	18	2472	17	2687	10
9	2852	27	3239	28	3291	15	2017	14
10	2603	16	1956	19	2488	15	2547	15
11	1145	12	2962	17	3474	27	1987	13
12	1651	14	2719	27	2124	13	1753	9
13	1554	20	1896	17	3654	20	1987	10
14	4060	27	2318	24	2019	15	2587	17
15	2067	13	6100	28	1698	14	1923	13
16	2337	13	2109	12	3912	21	1652	11

4.4.6. Appendix F: The raw data of Table 3.2.

Body mass, muscle mass, bone mineral content (BMC), bone area and bone mineral density (BMD) in adult transgenic and wild-type mice.

ID	Sex	Genotype	Body mass (g)	Muscle mass (g)	BMC (g)	Bone area (cm²)	BMD (g/cm³)
43	M	TG	22.8	17.5	0.35	6.86	0.0511
85	M	TG	24.1	18.3	0.368	6.94	0.053
946	M	TG	25.4	17.8	0.406	7.75	0.0524
954	M	TG	24	17.1	0.404	7.98	0.0506
964	M	TG	25.1	19.1	0.403	7.84	0.0514
77	M	TG	25.1	17.7	0.389	7.03	0.0553
78	M	TG	23.8	18.4	0.402	6.6	0.0609
935	M	TG	24.7	19	0.383	7.97	0.048
952	M	TG	24	17.1	0.396	7.74	0.0511
55	F	TG	16.8	12.2	0.248	6.01	0.0413
87	F	TG	20.4	15	0.313	6.78	0.0462
944	F	TG	20.3	15.1	0.41	7.58	0.0541
948	F	TG	21.5	15.3	0.412	7.83	0.0526
76	F	TG	19.2	13.3	0.343	6.96	0.0493
938	F	TG	20	14.3	0.345	7.1	0.0486
939	F	TG	20	14.7	0.348	7.19	0.0484
940	F	TG	18.9	14.1	0.334	7.16	0.0466
941	F	TG	22.5	16.5	0.365	7.51	0.0486
980	F	TG	20	14.8	0.367	7.19	0.049
981	F	TG	17.7	12.5	0.317	7.24	0.0438
983	F	TG	20.1	14.2	0.32	6.89	0.0464
987	F	TG	20.7	14.6	0.35	7.22	0.0485
992	F	TG	18.6	13.6	0.3	7	0.0429

44	M	WT	19.9	15	0.287	6.74	0.0426
45	M	WT	19.4	13.5	0.256	6.25	0.0409
46	M	WT	19.2	13	0.277	6.59	0.0421
86	M	WT	23.2	16.9	0.325	6.75	0.0481
949	M	WT	23.8	17.4	0.457	8.52	0.0537
951	M	WT	22.6	16.1	0.379	7.61	0.0498
955	M	WT	22.4	15.7	0.386	7.85	0.0491
958	M	WT	23.1	17	0.395	7.53	0.0525
962	M	WT	26	17.9	0.37	7.88	0.0469
80	M	WT	24.8	16.1	0.359	7.24	0.0496
81	M	WT	22.6	17.2	0.353	6.5	0.0543
942	M	WT	23.7	17.3	0.357	7.69	0.0464
54	F	WT	17.6	12.6	0.251	6.19	0.0406
56	F	WT	17.2	11.7	0.231	5.99	0.0386
58	F	WT	15.5	11.6	0.215	5.84	0.0369
59	F	WT	15	10.7	0.209	5.68	0.0367
60	F	WT	15	10.9	0.199	5.43	0.0367
82	F	WT	17.7	12.6	0.27	6.3	0.0428
83	F	WT	18.9	13.7	0.3	6.72	0.0447
84	F	WT	19.1	13.9	0.32	6.68	0.0479
945	F	WT	18.4	13.1	0.338	6.93	0.0488
947	F	WT	21.5	15.5	0.449	9.9	0.0454
950	F	WT	18.1	13.3	0.398	7.87	0.0506
79	F	WT	20.3	15.4	0.352	6.77	0.052
936	F	WT	17.4	12.3	0.319	6.67	0.0477
943	F	WT	18.4	13.1	0.313	7.1	0.0441
985	F	WT	17.1	12.2	0.292	6.71	0.0436
993	F	WT	17.6	12.6	0.288	6.61	0.0436

4.4.7. Appendix G: The raw data of Figure 3.7.

Trabecular bone volume and tissue volume in sagittal section of femur bone of adult transgenic and wild-type mice.

ID	Sex	Genotype	Trabecular bone volume (μm^2)	Tissue volume (μm^2)
103	M	WT	320	2372
103-2	M	WT	270	2481
105	M	WT	210	1993
106-2	M	WT	250	2840
112-2	M	WT	300	1881
113	M	WT	200	1741
113-2	M	WT	187	1935
125-2	F	WT	140	2462
125-3	F	WT	250	2256
129	F	WT	190	2018
105-2	F	WT	129	2031
106-4	F	WT	136	1924
107-2	F	WT	312	1705
112-3	F	WT	280	1874
101-4	M	TG	210	1230
106	M	TG	490	2640
112	M	TG	400	2087
124-3	M	TG	470	1639
124-4	M	TG	410	1998
125	M	TG	189	1960
127-2	M	TG	210	2110

101-3	M	TG	381	1560
130	F	TG	289	2036
130-2	F	TG	249	1494
127	F	TG	270	1605
103-3	F	TG	379	2553
107-3	F	TG	340	1674
128	F	TG	367	2037
131	F	TG	251	1657
131-2	F	TG	367	2394